CENTRAL RESEARCH LIBRARY
DOCUMENT COLLECTION

MARTIN MARIETTA ENERGY SYSTEMS LIBRARIES
3 4456 0349585 8

ORNL 1624
Engineering

THE NATURE OF THE FLOW OF ORDINARY FLUIDS IN A THERMAL CONVECTION HARP

D. C. Hamilton
F. E. Lynch
L. D. Palmer

CENTRAL RESEARCH LIBRARY
DOCUMENT COLLECTION

LIBRARY LOAN COPY

DO NOT TRANSFER TO ANOTHER PERSON

If you wish someone else to see this document, send in name with document and the library will arrange a loan.

OAK RIDGE NATIONAL LABORATORY
OPERATED BY
CARBIDE AND CARBON CHEMICALS COMPANY
A DIVISION OF UNION CARBIDE AND CARBON CORPORATION

POST OFFICE BOX P
OAK RIDGE, TENNESSEE

ORNL 1624

Copy No. 4

Contract No. W-7405-eng-26

Reactor Experimental Engineering Division

THE NATURE OF THE FLOW OF ORDINARY FLUIDS IN A THERMAL CONVECTION HARP

D. C. Hamilton
F. E. Lynch
L. D. Palmer

DATE ISSUED

FEB 23 1954

OAK RIDGE NATIONAL LABORATORY
Operated by
CARBIDE AND CARBON CHEMICALS COMPANY
A Division of Union Carbide and Carbon Corporation
Post Office Box P
Oak Ridge, Tennessee

MARTIN MARIETTA ENERGY SYSTEMS LIBRARIES

3 4456 0349585 8

ORNL 1624
Engineering

INTERNAL DISTRIBUTION

1. C. E. Center
2. Biology Library
3. Health Physics Library
4-5. Central Research Library
6. Reactor Experimental Engineering Library
7. ANP Reports Office
8-12. Laboratory Records Department
13. Laboratory Records, ORNL R.C.
14. C. E. Larson
15. L. B. Emlet (K-25)
16. J. P. Murray (Y-12)
17. A. M. Weinberg
18. E. H. Taylor
19. E. D. Shipley
20. C. E. Winters
21. J. A. Lane
22. F. C. VonderLage
23. R. C. Briant
24. J. A. Swartout
25. S. C. Lind
26. F. L. Culler
27. A. H. Snell
28. A. Hollaender
29. M. T. Kelley
30. C. P. Keim
31. R. S. Livingston
32. J. H. Frye, Jr.
33. W. J. Fretague
34. G. H. Clewett
35. K. Z. Morgan
36. T. A. Lincoln
37. A. S. Householder
38. C. S. Harrill
39. D. W. Cardwell
40. D. S. Billington
41. E. M. King
42. R. N. Lyon
43. A. J. Miller
44. R. B. Briggs
45. A. S. Kitzes
46. O. Sisman
47. R. W. Stoughton
48. C. B. Graham
49. W. R. Gall
50. H. F. Poppendiek
51. S. E. Beall
52. J. P. Gill
53. D. D. Cowen
54. J. O. Bradfute
55. A. P. Fraas
56. H. W. Hoffman
57. P. R. Kasten
58. N. F. Lansing
59. P. C. Zmola
60. G. C. Williams
61. M. J. Skinner
62. W. H. Jordan
63. M. W. Rosenthal
64. W. D. Powers
65-114. D. C. Hamilton
115-119. F. E. Lynch
120-124. L. D. Palmer
125. E. G. Bohlmann
126. J. C. Greiss
127. J. L. English
128. H. C. Claiborne
129. L. G. Alexander
130. E. C. Miller
131. W. O. Harms
132. D. G. Thomas
133. M. A. Beckner
134. W. K. Ergen
135. C. B. Mills
136. M. T. Robinson
137. N. D. Greene
138. G. M. Adamson
139. R. G. Affel
140. E. S. Bettis
141. E. P. Blizard
142. A. D. Callihan
143. W. G. Cobb
144. S. I. Cohen
145. C. P. Coughlen
146. G. A. Cristy
147. J. Y. Estabrook
148. W. R. Grimes
149. J. R. Johnson
150. G. W. Keilholtz
151. F. Kertesz
152. W. D. Manly
153. E. R. Mann
154. W. B. McDonald
155. J. L. Meem
156. E. J. Murphy
157. W. W. Parkinson
158. D. F. Salmon
159. H. W. Savage
160. J. M. Warde
161. C. G. Lawson
162. W. M. Breazeale (consultant)
163. R. A. Charpie

EXTERNAL DISTRIBUTION

164. W. J. Larkin, USAEC, Oak Ridge
165. R. F. Bacher, California Institute of Technology
166-409. Copies given distribution as shown in TID-4500 under Engineering

DISTRIBUTION PAGE TO BE REMOVED IF REPORT IS GIVEN PUBLIC DISTRIBUTION

TABLE OF CONTENTS

PAGE

SUMMARY 4

INTRODUCTION 6

NOMENCLATURE 10

PREDICTION OF THE REYNOLDS MODULUS FOR THE LAMINAR FLOW REGIME 14

The Dynamic Equation for a Thermal Convection Harp..... 14

Calculation of $\Delta\Phi_b$ by Numerical Solution of the Heat Conduction Equation 16

The method 17
The procedure 19

Prediction of the Reynolds Modulus 21

RESULTS AND DISCUSSION 24

The Velocity Structure 26

The Temperature Structure 34

Evidences of Turbulence 40

Comparison of Measured and Predicted Reynolds Moduli 47

CONCLUSIONS 50

REFERENCES 53

APPENDIX 54

Apparatus and Procedure 55

Harp arrangement 55
Instrumentation for velocity measurements..... 57
Instrumentation for temperature measurements 60
Experimental procedure 63

Treatment of Velocity Data 64

SUMMARY

Experiments were conducted to obtain information on the nature of the flow and heat transfer of ordinary fluids in a thermal convection harp. In addition, the mean flow rate, or Reynolds modulus, was predicted for each of the experiments by use of the wall temperature data and a numerical solution of the laminar flow heat conduction equation.

The harp used in this experiment was a loop consisting of four interconnected straight pieces of tubing, two of which were vertical and two of which were essentially horizontal. Heat was added to one of the vertical legs and removed from the other; the two horizontal legs were maintained essentially adiabatic. The harp was constructed of 0.7 inch I.D. Pyrex tubing and had an effective height of 2.5 feet. Tap water was used as the primary fluid. Velocity profiles were obtained from observations of suspended particles in the water. Specially designed thermocouple probes permitted measurement of the wall and fluid temperatures.

In forced convection the flow is characterized by the value of the Reynolds modulus, while in free convection it is characterized by the value of the Grashof modulus. The flow in a thermal convection harp is superimposed-free-and-forced-flow and both moduli are needed to define the flow system. In the present experiment the Reynolds modulus was varied from 50 to 270 while the Grashof modulus was varied from 2×10^4 to 67×10^4.

The investigation revealed that, on the basis of the velocity structure, the heat transfer rate, and the flow regime, the flow and heat transfer of ordinary fluids in a thermal convection harp having adiabatic horizontal legs is more nearly characteristic of free convection than of forced convection. Above the critical value of the Grashof modulus, which was about 10^5, the flow deviated markedly from the laminar structure. The corresponding value of the Reynolds modulus was about 100. The predicted and measured values of the Reynolds modulus agreed to within 30 percent where the flow was laminar. Above the critical value of the Grashof modulus, where the flow was transitional or turbulent, the method was not applicable and the agreement was unsatisfactory.

INTRODUCTION

On the basis of a cursory appraisal, the harp boiler or thermal convection harp appears to have several advantages as a dynamic corrosion testing device; the principle advantage seems to be the elimination of the pump. In order to evaluate the overall effectiveness of the device or to interpret the data obtained from it, the corrosion worker would need information concerning the velocity and temperature structure; a satisfactory method for determining the mean flow rate would also be desirable. The purpose of the present work is to furnish this information.

In reference 1, Hackett describes the mass transport problem that was encountered in the operation of the first mercury power plant cycle around 1925. The iron was removed from the hot tubes in the boiler and deposited on the walls of the cooler part of the circuit by the action of the flowing mercury; this resulted in choking or plugging in the cold tubes. Hackett mentions that A. J. Nerad and associates designed "harp boilers" that were used in a research program which resulted in the discovery that the transport of iron was satisfactorily inhibited by the addition of titanium and magnesium to the mercury. The details of the research of Nerad, et. al., were not published and the dynamic structure in their harps is not known. However, the information available about the harps from reference 1, together with the known physical properties of mercury, permits one to estimate that the value of Grashof modulus was sufficiently high to cause turbulent flow. A comparison of the physical properties and liquid temperature ranges for water and

mercury indicates that the highest Grashof modulus attainable with mercury is about 500 times greater than that attainable with water in the same system. For this reason the expected flow regime for water or other ordinary fluids (non-liquid-metals) is less certain.

The term, ordinary fluid, is used throughout the text to designate fluids having values of Prandtl modulus in the range from 1 to 100. In contrast to ordinary fluids, liquid metals are characterized by Prandtl moduli of approximately 0.01. The thermal structure of these two classes of fluids is markedly different in the turbulent flow regime and it is thus necessary to differentiate between the two classes in heat transfer systems.

The flow and heat transfer in a thermal convection harp is essentially a problem in convection heat transfer. It is natural, then, that the dimensionless moduli of convection are the significant parameters. Because the report is written principally for those interested in corrosion or mass transfer rather than for heat transfer specialists, the plan of presentation has been changed to focus the attention on the results as quickly as possible. For this reason the discussion of the experimental apparatus and procedure has been relegated to the appendix; thus, a brief description of the primary system is desirable here.

The harp used in this equipment is essentially the same as the harp boilers of Nerad; however, the design was modified to facilitate the measurements of fluid and wall temperatures and to make the system more amenable to analysis. The primary flow circuit, shown in Figure 1, consists essentially of a piece of 0.7 inch I.D. Pyrex tubing 79 inches long, bent in the form of a rectangular

UNCLASSIFIED
Dwg. 22730

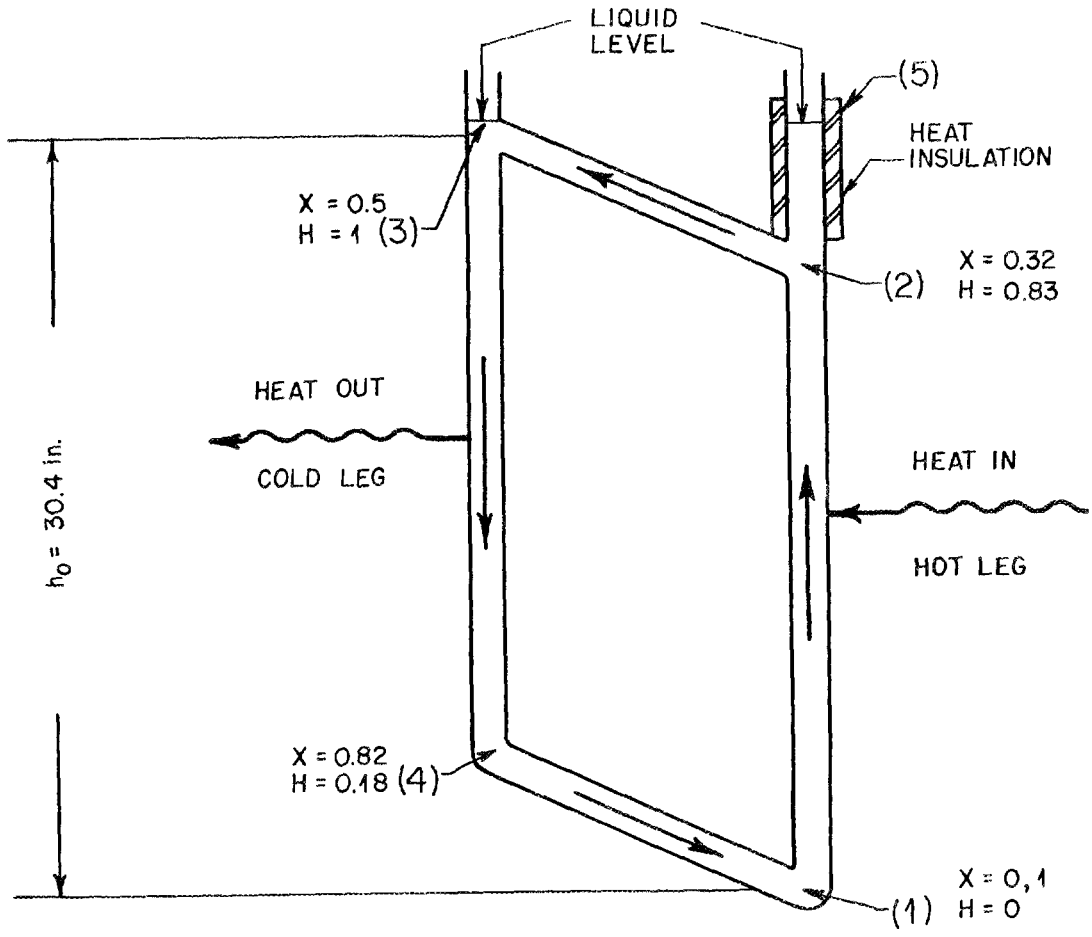

Fig. 1. Schematic Diagram of Primary Flow Circuit of Thermal Convection Harp. (Showing Coordinate Systems)

loop and inter-connected at its two ends. The loop described is indicated by the hot leg, (1) to (2), the upper connecting leg, (2) to (3), the cold leg, (3) to (4), and the lower connecting leg, (4) to (1). Throughout the report positions along the axis of the harp are designated by the values of the normalized axial coordinate, X. The values of X are indicated at each of the bends in the primary circuit. The extensions at the top of the hot leg, (2) to (5), and the cold leg, provide access for the thermocouple probes.

The velocity measurements were made by timing the paths of suspended droplets in the water. The authors had previously used this technique in another free convection experiment. It was not believed desirable in this experiment to refine the technique to include high speed photography. The visual technique used here is not applicable for highly turbulent flow or for velocities greater than 200 feet per hour.

This report consists essentially of two parts. The first is an analytical method for predicting the Reynolds modulus in a harp from wall temperature data by a numerical solution of the laminar flow heat conduction equation. The second is the experimental measurements of the velocity, turbulence, and temperature structures in the harp.

NOMENCLATURE

Dimensionless Moduli

Φ = $\frac{\theta}{\theta_{w,max}}$ - normalized temperature function

Φ_w = wall temperature

$\Delta\Phi_b$ = $\oint \Phi_m(H)\, dH = \left[\int_0^1 \Phi_m(H)\, dH\right]_{\text{hot leg}} - \left[\int_0^1 \Phi_m(H)\, dH\right]_{\text{cold leg}}$

normalized buoyant temperature difference

Gr_d = $\left(\frac{d^3\beta g}{\nu^2}\right) \theta_{w,max}$ - Grashof modulus based on d

Gr_y = $\left(\frac{y^3\beta g}{\nu^2}\right) \theta_{w,max}$ - Grashof modulus based on y

Gz = $RePr\,\frac{d}{L}$ - Graetz modulus (note that Graetz modulus is more often defined as $\frac{\pi}{4}\,RePr\,\frac{d}{L}$)

Nu = $\frac{hd}{k}$ Nusselt modulus

Re = $\frac{u_m d}{\nu}$ Reynolds modulus

Pr = $\frac{\nu}{\alpha}$ Prandtl modulus

Throughout this report the subscript m indicates that a mean or average has been taken. In all cases it indicates an averaging process over the radial coordinate in the following manner:

$$V_m(X) = \int_0^1 V(R,X)\, 2RdR$$

Lower Case Letters

d	inside diameter of primary circuit ($d = 0.695$ inches); also differential operator.
f	functional operator
g	acceleration of gravity (ft./hr.^{2})
g_o	dimensional constant = 4.17×10^8 (ft. lb./lb. hr.^{2})
h	vertical distance above the lowest point of the centerline of primary system (ft.). Convective heat transfer coefficient (B/hr. ft.^{2} ^oF)
h_o	total height of primary system (2.5 ft.)
k	thermal conductivity - (B/hr. ft. ^oF)
n	radial position in finite difference grid (also used to indicate number of velocity observations).
p	pressure - (lb./ft.^{2})
r	radial coordinate (ft.)
r_o	maximum radius of system = $\frac{d}{2}$ (ft.)
s	axial position in finite difference grid.
t	temperature (^oF)
t_f	mean fluid temperature used for evaluating fluid properties (^oF) $\left(t_f = t_{w,min} + \frac{\theta_{w,max}}{2}\right)$
$t_{w,min}$	the minimum inside wall temperature for a given Data Set (occurred at $X \cong 0.81$) (^oF)
u	fluid velocity (ft./hr.)
x	axial coordinate measured along centerline and starting at bottom of hot leg (ft.)
y	axial coordinate measured along centerline and starting at top of cold leg (ft.)

Upper Case Letters

A	flow area - (ft.^{2})
B	factors in finite difference equation
C	constant
C_p	heat capacity - (Btu/lb. ^oF)
F	radius distribution function used in Appendix; also used for fluid friction term $F = \lambda \frac{L}{d} \frac{\rho_m (u_m)^2}{2g_o}$ (ft. lb./ft.^{3})
G	velocity distribution function used in Appendix
H	normalized vertical coordinate = $\frac{h}{h_o}$ (see Figure 1)
K	factors defined in Equations 19 and 20
L	distance around the primary circuit measured along the centerline (L = 78.9 inches)
N_R	number of radial subdivisions used in the numerical solution
N_X	number of axial subdivisions used in the numerical solution
R	normalized radial coordinate $R = \frac{r}{r_o}$
U(R)	dimensionless velocity = $\frac{u}{u_m}$
W	work done by fluid - (ft. lb./ft.^{3})
X	normalized axial coordinate = $\frac{x}{L}$ (see Figure 1)

Combined Upper Case Letters

K.E. kinetic energy term in Equation (1)

$$K.E. = (U^3)_m \frac{\rho_m (u_m)^2}{2g_o} \text{ (ft. lb./ft.}^3\text{)}$$

P.E. potential energy term in Equation (1)

$$P.E. = \rho_m \frac{g}{g_o} h \text{ (ft. lb./ft.}^3\text{)}$$

Greek Letters

α molecular thermal diffusivity - (ft.^{2}/hr.)

β thermal coefficient of expansion of fluid - (1/°F)

δ free convection boundary layer thickness (ft.)

θ temperature level above base temperature $\theta = t - t_{w,min.}$ (°F)

θ_w inside wall temperature level (°F)

$\theta_{w,max} = t_{w,max} - t_{w,min}$ - the maximum variation in the inside wall temperature (°F)

λ friction factor $\lambda = \dfrac{\Delta p_f}{\frac{L}{d} \frac{\rho u_m^2}{2g_o}}$

where Δp_f is the pressure drop due to friction

μ dynamic viscosity - (lb./ft. hr.)

ν kinematic viscosity - (ft.^{2}/hr.)

ξ radial distribution factor used in Appendix

ρ mass density - (lb./ft.^{3})

ω angular coordinate in the cylindrical coordinate system used here

PREDICTION OF THE REYNOLDS MODULUS FOR THE LAMINAR FLOW REGIME

In the application of a thermal convection harp it would be desirable to know the magnitude of the Reynolds modulus and the amount of variation of the Reynolds modulus during the course of an experiment. For the case where the flow is laminar this information can be obtained from wall temperature measurements and a numerical analysis. In order to predict the Reynolds modulus by such an analysis three quantities must be known; these are the Grashof modulus, the friction factor, and the buoyant temperature difference. The Grashof modulus can be computed from the wall temperature data and the fluid properties; in the present analysis, the friction factor for isothermal laminar flow in long, straight pipes of circular cross section will be assumed. With these two quantities known the dynamic equation for a thermal convection harp is reduced to a relationship between the Reynolds modulus and the normalized buoyant temperature difference. The prediction of the Reynolds modulus from wall temperature data is then simplified to the problem of the calculation of the buoyant temperature difference.

The Dynamic Equation for a Thermal Convection Harp

The dynamic equation for forced flow through a duct of uniform area is:

$$dp + d(K.E.) + dW + d(P.E.) + dF = 0 \quad . \; . \; . \; . \; . \; . \; . \; . \; . \quad (1)$$

Since the system of interest here is a closed loop, the integration of the equation around the loop is useful.

$$\oint dp = 0$$

$$\oint d(K.E.) \neq 0$$

The kinetic energy term above, although not zero, was assumed to be negligible for the present system. Since there is no pump in the system the work term is zero. Equation (1) then reduces to a relationship between the potential energy and the friction terms, or

$$-\oint \rho_m(X) \frac{g}{g_o} dh = \lambda \frac{L}{d} \frac{\rho_f u_m^2}{2g_o} \quad \ldots\ldots\ldots\ldots \quad (2)$$

From the definition of β get:

$$\frac{\rho_m(X)}{\rho_f} = 1 - \beta \theta_{w,max}(\Phi_m(X) - \Phi_f) \quad \ldots\ldots\ldots \quad (3)$$

Putting (3) in (2) and rearranging, get;

$$Re = \left(\frac{2}{\lambda} \frac{h_o}{L} Gr_d \Delta\Phi_b\right)^{1/2} \quad \ldots\ldots\ldots\ldots \quad (4)$$

Equation (4) is valid for a thermal convection harp in either turbulent or laminar flow. Consider a system in which the geometry and fluid properties are fixed; Equation (4) then becomes;

$$Re = C_1 \left(\theta_{w,max} \frac{\Delta\Phi_b}{\lambda}\right)^{1/2} \quad \ldots\ldots\ldots \quad (4a)$$

From Equation (4a) it is seen that, if the friction factor, λ, is known, and if the normalized buoyant temperature difference, $\Delta\Phi_b$, can be computed, then the equation is reduced to a relationship between the Reynolds modulus, Re, and the maximum wall temperature difference, $\theta_{w,max}$.

For isothermal turbulent flow in long, smooth, straight pipes the friction factor can be expressed over the lower range of Reynolds moduli as;

$$\lambda = 0.184\ Re^{-0.2} \quad \ldots\ldots\ldots\ldots\ldots \quad (5)$$

When this expression is employed Equation (4) becomes;

$$Re = \left(10.87\ \frac{h_o}{L}\ Gr_d\ \Delta\Phi_b\right)^{0.555} \quad \ldots\ldots\ldots\ldots \quad (6)$$

The friction factor expression for the isothermal laminar flow through a long, straight pipe of circular cross-section is;

$$\lambda = 64/Re \quad \ldots\ldots\ldots\ldots\ldots \quad (7)$$

Putting (7) in (4) get;

$$Re = \frac{1}{32}\ \frac{h_o}{L}\ Gr_d\ \Delta\Phi_b \quad \ldots\ldots\ldots\ldots\ldots \quad (8)$$

Equation (8) is the dynamic equation for a thermal convection harp in laminar flow. The friction factor postulated does not include the losses around the bends nor the influence of the free convection entrance regions on the friction. These idealizations would tend to cause the Reynolds modulus predicted on the basis of Equation (8) to be too large.

Calculation of $\Delta\Phi_b$ by Numerical Solution of the Heat Conduction Equation

In order to employ Equation (8) to predict the Reynolds modulus in a thermal convection harp one must be able to determine the value of $\Delta\Phi_b$. The method suggested here involves a numerical solution of the heat conduction equation

for laminar flow. After the method of calculation has been developed from the basic equation the calculation procedure used in the present work will be discussed.

The method

The laminar flow heat conduction equation for flow in a circular pipe is given below:

$$U(X,R)\,\frac{\partial\Phi(X,R)}{\partial X} = \frac{4}{Gz}\left(\frac{d^2}{4L^2}\,\frac{\partial^2\Phi(X,R)}{\partial X^2} + \frac{\partial^2\Phi(X,R)}{\partial R^2} + \frac{1}{R}\,\frac{\partial\Phi(X,R)}{\partial R}\right) \quad . \; . \quad (9)$$

For the present system, due to the relatively large value of $Gz\left(\frac{L}{d}\right)^2$, the axial conduction term can be neglected; in addition, to simplify the analysis, the velocity will be postulated to be a function only of radius. Thus, Equation (9) becomes:

$$U(R)\,\frac{\partial\Phi(X,R)}{\partial X} = \frac{4}{Gz}\left(\frac{\partial^2\Phi(X,R)}{\partial R^2} + \frac{1}{R}\,\frac{\partial\Phi(X,R)}{\partial R}\right) \quad . \; . \; . \; . \; . \; . \; . \; . \quad (10)$$

The velocity profile observed in this work did change with X; this variation could have been included in the numerical analysis but the results of this work indicate that it was not necessary. The finite difference form of Equation (10) is:

$$\Phi(s+1,n) = B_{n-1}\,\Phi(s,n-1) + B_{n+1}\,\Phi(s,n+1) + B_n\Phi(s,n) \quad . \; . \; . \; . \quad (11)$$

where
$$B_{n-1} = \frac{4\ N_R^2}{Gz\ N_X}\ \frac{1}{U(n)}\left(1 - \frac{1}{2N_R\ R(n)}\right)$$

$$B_{n+1} = \frac{4\ N_R^2}{Gz\ N_X}\ \frac{1}{U(n)}\left(1 + \frac{1}{2N_R\ R(n)}\right) \qquad (11a)$$

$$B_n = 1 - \frac{8\ N_R^2}{Gz\ N_X\ U(n)}$$

N_X - number of axial subdivisions used

N_R - number of radial subdivisions used

The symbols s and n indicate the axial and radial locations respectively, in the finite difference coordinate grid. From Equation (11) it is clear that one computes the temperature for one axial increment ahead, (s+1), from the known values of the temperatures for the elements at the axial locations (s). For the discussion to follow the fluid properties and the geometry of the harp system will be considered fixed. The Graetz modulus can then be considered to be proportional to the Reynolds modulus. The solution to Equation (10), or (11), is of the form:

$$\Phi(X,R) = f_1\left(C_1\ Re,\ U(R),\ \Phi_w(X)\right) \quad . . . . . .(12)$$

After $\Phi(X,R)$ is known from the solution of Equation (11) the mean temperature can be computed.

$$\Phi_m(X) = \int_0^1 2R\ \Phi(X,R)\ dR \quad . . . . . \quad (13)$$

After transforming the mean temperature from the axial coordinate, X, to the vertical coordinate, H, the buoyant temperature difference can be obtained.

$$\Delta\Phi_b = \oint \Phi_m(H)\, dH \quad . \; . \; . \; . \; . \; . \; . \; . \; . \; . \; . \qquad (14)$$

Thus

$$\Delta\Phi_b = f_2\left(C_1\, Re,\ U(R),\ \Phi_w(X)\right) . \; . \; . \; . \; . \; . \; . \; . \qquad (15)$$

It should be emphasized here that Φ and U are normalized variables and express the form, not the absolute values, of the temperature and the velocity profiles. In computing $\Delta\Phi_b$ the wall temperature, $\Phi_w(X)$, is known from experimental measurements. Then, for each set of postulated values for U(R) and C_1 Re, a unique value for $\Delta\Phi_b$ is obtained.

The procedure

The solution to Equation (11) was obtained for thirty different conditions; that is, for five different wall temperature distributions, three different values of Graetz modulus and two velocity profiles. The resulting values of $\Delta\Phi_b$ are given in Table 2 in RESULTS AND DISCUSSION. The solutions were obtained on the ORNL high speed computer, the ORACLE*. The harp was divided into 10 radial and 200 axial subdivisions. To begin the problem a temperature distribution was postulated at some axial location; say at X = 0. In the present case it was postulated that the fluid temperature was uniform and equal to the wall temperature at X = 0.

Then, for the conditions being considered, the B factors were computed for each radial position, or value of n, from Equations (11a). There was one

---

*The authors are indebted to Miss Phyllis Brown of the ORNL Mathematics Panel for having done the coding and programming of this problem.

exception; the equations do not apply for the element at the center of the pipe. To satisfy symmetry the temperature gradient should be equal to zero at the center; for this reason the center element was assumed to have the same temperature as the element radially adjacent to it. Then, with the values of the B's known and the wall temperatures tabulated the temperatures were computed for the entire circuit around the harp by use of Equation (11). When the entire length had been traversed the temperatures at X = 1 were compared to the temperatures that were postulated at X = 0 when the computation was begun. Ideally, if the initially postulated profile at X = 0 had been correct, the profile at X = 1 would be identical to it. Or, if the process is repeated for many cycles, the solution will converge to the ideal case mentioned above. In the present report the machine was set to compare the profile at X = 0 for successive cycles; when the maximum difference in the temperatures of these profiles was less than 0.01 degree Fahrenheit the calculation was considered satisfactory. The machine was also set to integrate each profile, in accordance with Equation (13), for the mean temperature.

Two of the points were checked on a hand calculator by the authors using a grid of 7 radial and 50 axial divisions. The results agreed well with the machine calculations. In this case a concerted effort was made to guess the starting profile with as great an accuracy as possible. Only five cycles were necessary in order to obtain satisfactory convergence.

The normalized buoyant temperature difference was obtained by graphical integration of Equation (14) using the mean temperatures, $\Phi_m(X)$, from the machine calculations.

Prediction of the Reynolds Modulus

The Reynolds modulus is predicted by the solution of the dynamic Equation (8) and the heat conduction Equation (15). Since $\Delta\Phi_b$ is dependent on Re in Equation (15) and Re is dependent on $\Delta\Phi_b$ in Equation (8), a repeated-trial technique is necessary.

$$Re = \left(\frac{1}{32}\frac{h_o}{L} Gr_d\right)\Delta\Phi_b \quad . . . . . \quad (8)$$

$$\Delta\Phi_b = f_2\left(C_1 Re,\ U(R),\ \Phi_w(X)\right) \quad . . . . . \quad (15)$$

For a particular system, after the wall temperatures have been measured, the factors $\frac{h_o}{L}$, Gr_d, C_1, and $\Phi_w(X)$ are known and the equations become:

$$Re = C_2\Delta\Phi_b \quad . . . . . \quad (8a)$$

and $$\Delta\Phi_b = f_3(Re,\ U(R)) \quad . . . . . \quad (15a)$$

In order to solve (15a) a value for U(R) must be postulated; for this discussion let it be postulated that the velocity is uniform; that is:

$$U(R) = 1 \quad . . . . . \quad (16)$$

The system to be solved now becomes

$$\Delta\Phi_b = f_4\ (Re_{post.}) \quad . . . . . \quad (15b)$$

and $$Re_{cal.} = C_2\Delta\Phi_b \quad . . . . . \quad (8a)$$

To obtain the repeated-trial solution, a value of $Re_{post.}$ is postulated in (15b) from which $\Delta\Phi_b$ is computed. This $\Delta\Phi_b$, when put in (8a), yields a value

of $Re_{cal.}$. From repetitions of this procedure a graph can be plotted of $Re_{cal.}$ versus $Re_{post.}$. The intersection of this line with the equation, $Re_{cal.} = Re_{post.}$, is the desired solution. In Figure 2 the solution is shown for the conditions of "Data Set C." The wall temperature data for this case are given in RESULTS AND DISCUSSION. The solution was obtained for two values of U(R) that were believed to be representative of the extremes which might be expected in the actual system. For this case the Reynolds modulus was measured as 111. The predicted values were 146 and 154 for postulated velocity distributions of $U(R) = 1$ and $U(R) = 6R(1-R)$, respectively.

UNCASSIFIED
Dwg. 22731

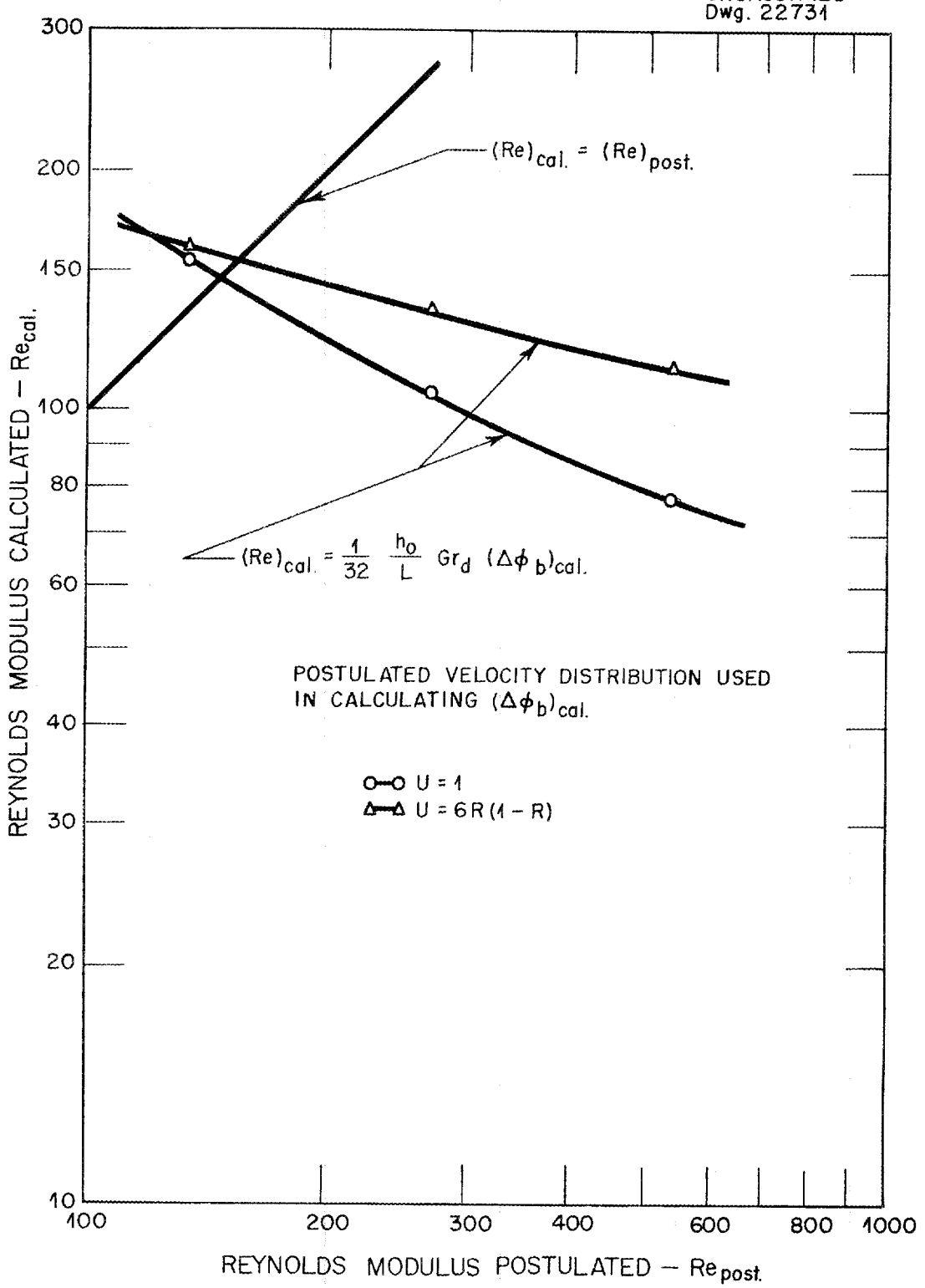

Fig. 2. Graphical Solution for the Predicted Value of Reynolds Modulus (For the Conditions of Data Set C)

RESULTS AND DISCUSSION

The experiments described in this report were performed for five different thermal and dynamic configurations of the system; these, for convenience, will be called Data Sets. In Table I the range of the important variables is given for each of the Data Sets. For the benefit of those readers who are not familiar with the meaning of the various dimensionless moduli used in heat transfer these moduli have been grouped, in Table I, according to flow, thermal driving force, and fluid properties. Thus, in a given experiment, where the fluid properties and the important dimensions are held constant the Reynolds modulus and the Graetz modulus are proportional to the mean velocity. Similarly, the Grashof modulus is proportional to the temperature difference or the thermal driving force causing the flow.

The experiments were performed in four separate stages as follows: First, for the conditions of Data Sets B, C, D, and E, wall temperature measurements were made and the velocity profiles were measured for the axial position designated by X equal to 0.677. Second, the optical device used in the velocity measurements was moved to an axial position corresponding to X equal to 0.555; then velocity profiles and wall temperature measurements were made for conditions of Data Sets A and C. Third, for the conditions of Data Sets D and E, fluid temperature profiles were measured at the five positions corresponding to values of X equal to 0.076, 0.2155, 0.53, 0.63, and 0.794. Finally, the apparatus was adjusted so that the velocity structure over the entire length of

TABLE I

RANGE OF VARIABLES

DATA SET	FLOW				Thermal Driving Force Causing Flow		Fluid Properties	
	OBSERVED FLOW REGIME	Mean Velocity	Reynolds Modulus	Graetz Modulus	Maximum Wall Temperature Difference	Grashof Modulus	Mean Fluid Temperature	Prandtl Modulus
		u_m $\frac{ft.}{hr.}$	$Re = \frac{u_m d}{\nu}$	$G_z = \frac{u_m d^2}{\alpha L}$	$\theta_{w,max}$ (°F)	$Gr_d = \frac{d^3 \beta g}{\nu^2} \theta_{w,max.}$	t_f (°F)	Pr
A	Laminar	32.3	49.2	2.96	3.3	2.1×10^4	70	6.82
B	Laminar	52.4	84.2	4.76	6.5	5.1×10^4	74	6.42
C	Laminar and Turbulent	72.1	111	6.59	11.9	8.0×10^4	71	6.73
D	Laminar and Turbulent	91.4	150	8.27	22.3	19.2×10^4	76.1	6.23
E	Laminar and Turbulent	133.7	272	11.73	38	67.2×10^4	93.4	4.9

the cold leg could be observed. With the apparatus so adjusted, qualitative observations of the velocity structure were made for the conditions of Data Sets A through E, inclusive.

In the discussion that follows the results are treated in four categories; these are the velocity structure, the temperature structure, the evidences of turbulence, and the comparison of predicted and measured Reynolds moduli.

The Velocity Structure

Before studying the flow in a free convection harp, it may be desirable to review the boundary layer flow for the case of free convection along a vertical plate as an aid in interpreting the velocity structure observed in the harp used in this experiment. Consider the case of a vertical plate submerged in a body of quiescent fluid. Let the plate be maintained at a uniform temperature that is lower than the uniform fluid temperature. As indicated in Figure 3 the vertical coordinate along the plate, y, will be considered to be equal to zero at the top of the plate. The fluid near the plate will be cooled by the plate and, due to the buoyant force caused thereby, this fluid will flow in a downward direction along the plate. At a given level the velocity profile in the boundary layer near the plate will be as shown in Figure 3. At the top of plate the boundary layer thickness is zero and the velocity is zero. As one procedes down the plate to greater values of y the boundary layer increases in thickness and the velocities increase. During the growth of the laminar boundary layer the flow remains laminar and the velocity profile retains essentially the same shape. After some critical value of y is reached the boundary layer becomes thick enough to become unstable and transition to a turbulent boundary layer

UNCLASSIFIED
Dwg. 22732

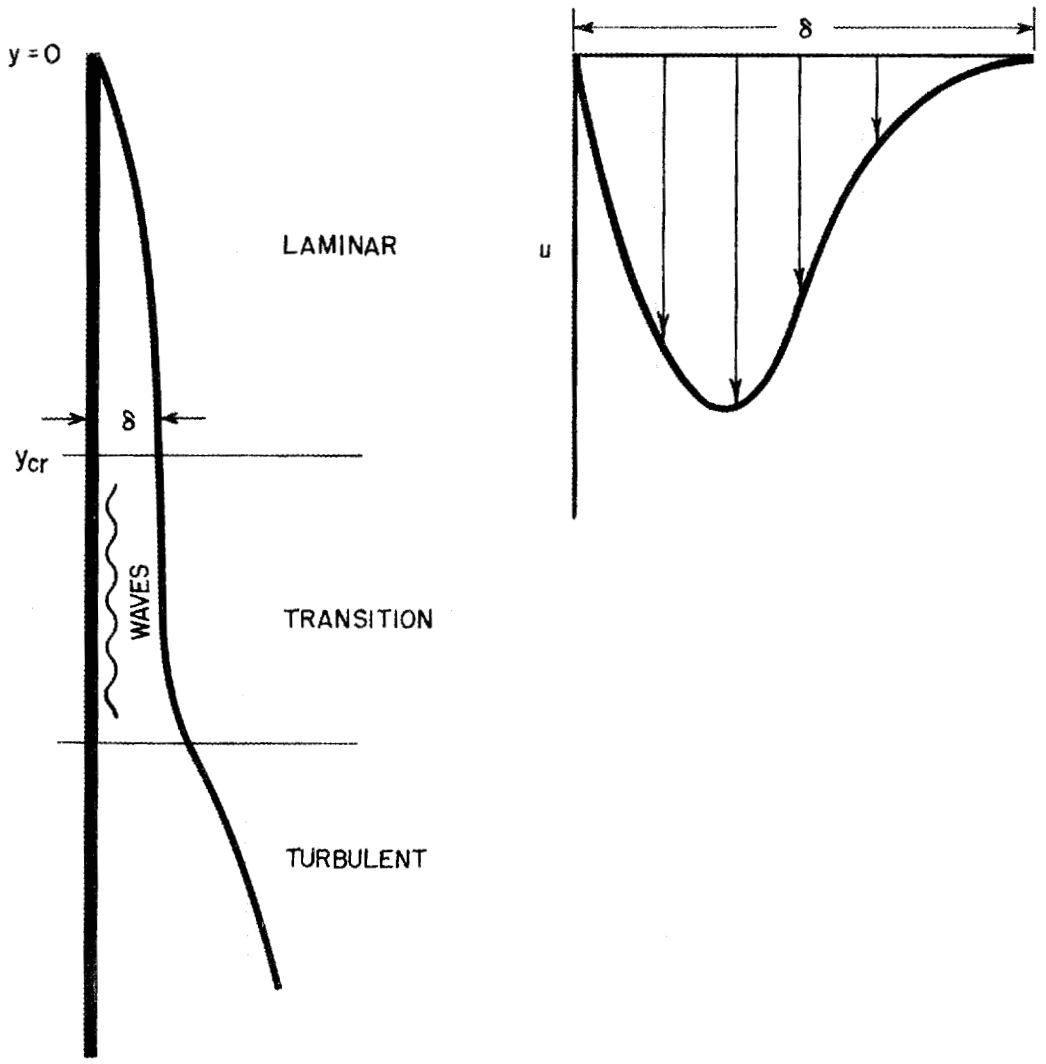

Fig. 3. Development of the Free Convection Boundary Layer Near A Cooled Vertical Plate.

begins. Beyond the transitional region the boundary layer becomes turbulent and the shape of the velocity profile and the law governing the growth of the boundary layer becomes different to that for the laminar boundary layer. The thickness of the laminar boundary layer, δ, at a distance y from the top of the plate is given by the following equation developed by Squire, reference 2.

$$\frac{\delta}{y} = 3.93 \left(\frac{Pr + 0.952}{Pr^2}\right)^{1/4} Gr_y^{-1/4} \quad \ldots\ldots\ldots \quad (17)$$

Multiplying both sides of Equation (17) by d and, solving for $\frac{y}{d}$, get:

$$\frac{y}{d} = \left(\frac{Pr^2}{Pr + 0.952}\right) \left(\frac{\frac{\delta}{d}}{3.93}\right)^4 Gr_d \quad \ldots\ldots\ldots \quad (17a)$$

At the entrance to the cold leg, where the boundary layer thickness is small compared to the pipe diameter, the boundary layer growth should be essentially identical to that in a flat plate system; however, as the boundary layer thickness increases, the influence of the circular geometry and of the forced flow continuity restriction would be expected to cause the boundary layer in a harp to grow at a faster rate. For the purpose of comparing the results of this experiment with Equation (17a) it was decided that the predicted location at which the boundary layer thickness was equal to d/4 would be more significant than a value of d/2. Now, for a Prandtl modulus equal to 6.8, the number of diameters down from the top of the plate at which the boundary layer thickness is equal to d/4 is computed as:

$$\left(\frac{y}{d}\right)_{\frac{\delta}{d} = \frac{1}{4}} \cong 10^{-4}\, Gr_d \quad \ldots\ldots\ldots \quad (17b)$$

The principal usefulness of Equation (17b) is to indicate that, from flat plate free convection boundary layer theory, one would expect to observe the velocity profile corresponding to the meeting of the laminar boundary layer in the cold leg to occur at greater values of y/d as Gr_d is increased.

In reference 3, Eckert and Soehngen, have measured the critical value of the Grashof modulus at which transition of the laminar boundary layer to a turbulent boundary layer for free convection may occur for the case of the flow over a vertical plate at a uniform temperature.

$$(Gr_y)_{critical} \cong 4 \times 10^8 \quad \ldots\ldots\ldots\ldots \quad (18)$$

Since $$Gr_y = Gr_d \left(\frac{y}{d}\right)^3$$

$$\left(\frac{y}{d}\right)_{critical} \cong \frac{34}{(Gr_d \times 10^{-4})^{1/3}} \quad \ldots\ldots\ldots \quad (18a)$$

Now let the flow observed in the cold leg of the thermal convection harp in the present experiment be considered. The velocity profiles in Figure 4 are the result of qualitative observations of the cold leg with the apparatus adjusted to illuminate the entire cold leg. As a result of having traversed the horizontal and adiabatic section of the harp and having made the turn at the top of the cold leg the fluid enters the cold leg with essentially uniform temperature and velocity. The flow in a thermal convection harp is properly classed as superimposed-free-and-forced-flow. Although the free flow component appears to be the dominant one, the forced flow aspect imposes an important restriction on the flow; this is the continuity principle. To satisfy this principle the <u>net</u> flow rate through any section of the system must be

UNCLASSIFIED
Dwg. 22733

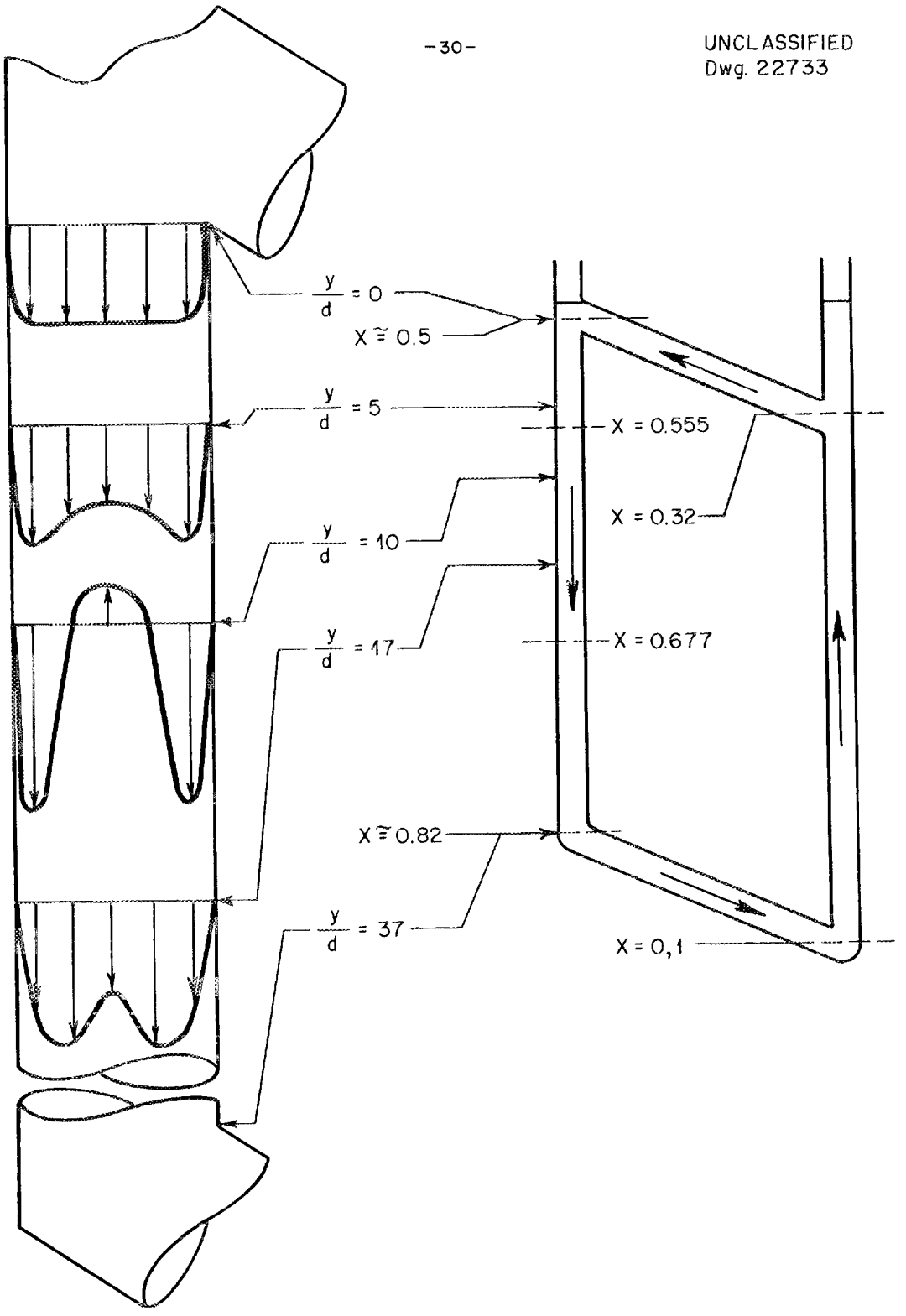

Fig. 4. Velocity Structure in the Cold Leg of a Thermal Convection Harp (For the Conditions of Data Set E)

the same. This means that, in the harp system at a given axial location, the velocities in the center of the pipe must decrease when the velocities near the wall increase; in some instances the center velocity would have to become negative to satisfy continuity. In Figure 4, at the location of $\frac{y}{d}$ equal to 5, or 5 diameters from the top of the cold leg, the free convection boundary layer has reached the center of the tube. At ten diameters down the tube negative velocities were observed in the central portions of the tube. At around 15 diameters the free convection boundary layer became turbulent and more efficient mixing of momentum and heat occurred causing the velocity profile to change to a more uniform distribution similar to that shown at 17 diameters. For the conditions of Data Sets A and B the center velocities never became negative and the change to turbulent free convection boundary layer never occurred. For the conditions of Data Sets C, D and E, the velocity profile sequence in Figure 4 is typical. The initiation of the negative center velocity occurred at a greater value of y as the Grashof modulus was increased; this is in agreement with Equation (17b). The transition to turbulence was observed to occur earlier for greater values of Grashof modulus; this is in agreement with Equation (18a).

In Figure 5 the measured velocity profiles in the upper portion of the cold leg are shown for the conditions of Data Sets A and D. In Figure 6, the velocity profiles for Data Sets B, C, D and E show the progressive growth of the laminar boundary layer that was described in Figure 4. Because of the low intensity of the light scattered from droplets near the center of the pipe it was always difficult to obtain data for the first three stations. This was

UNCLASSIFIED
Dwg. 22734

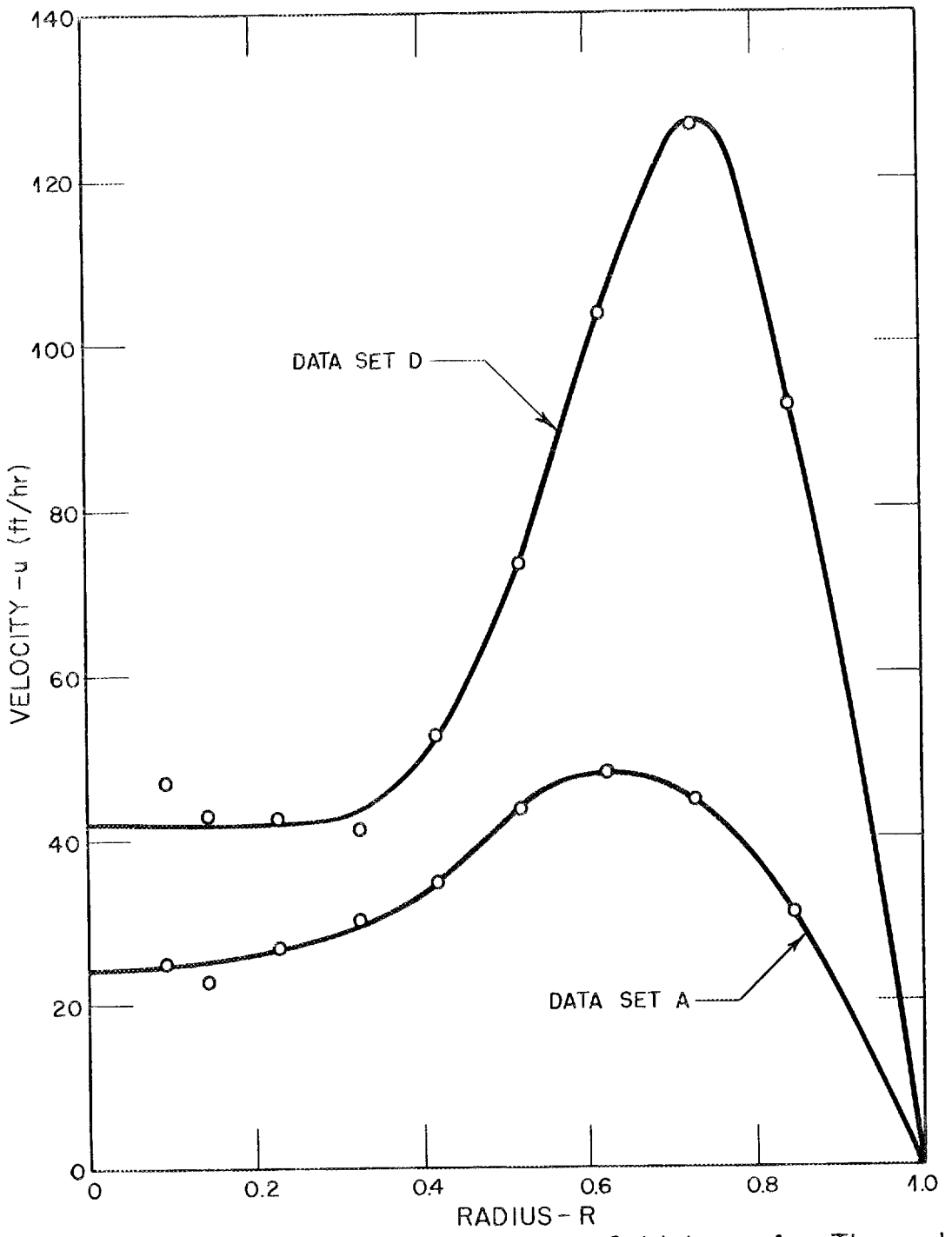

Fig. 5. Velocity Distribution in the Cold Leg of a Thermal Convection Harp at $X = 0.555$ $\left(\frac{y}{d} = 6\right)$

UNCLASSIFIED
Dwg. 22735

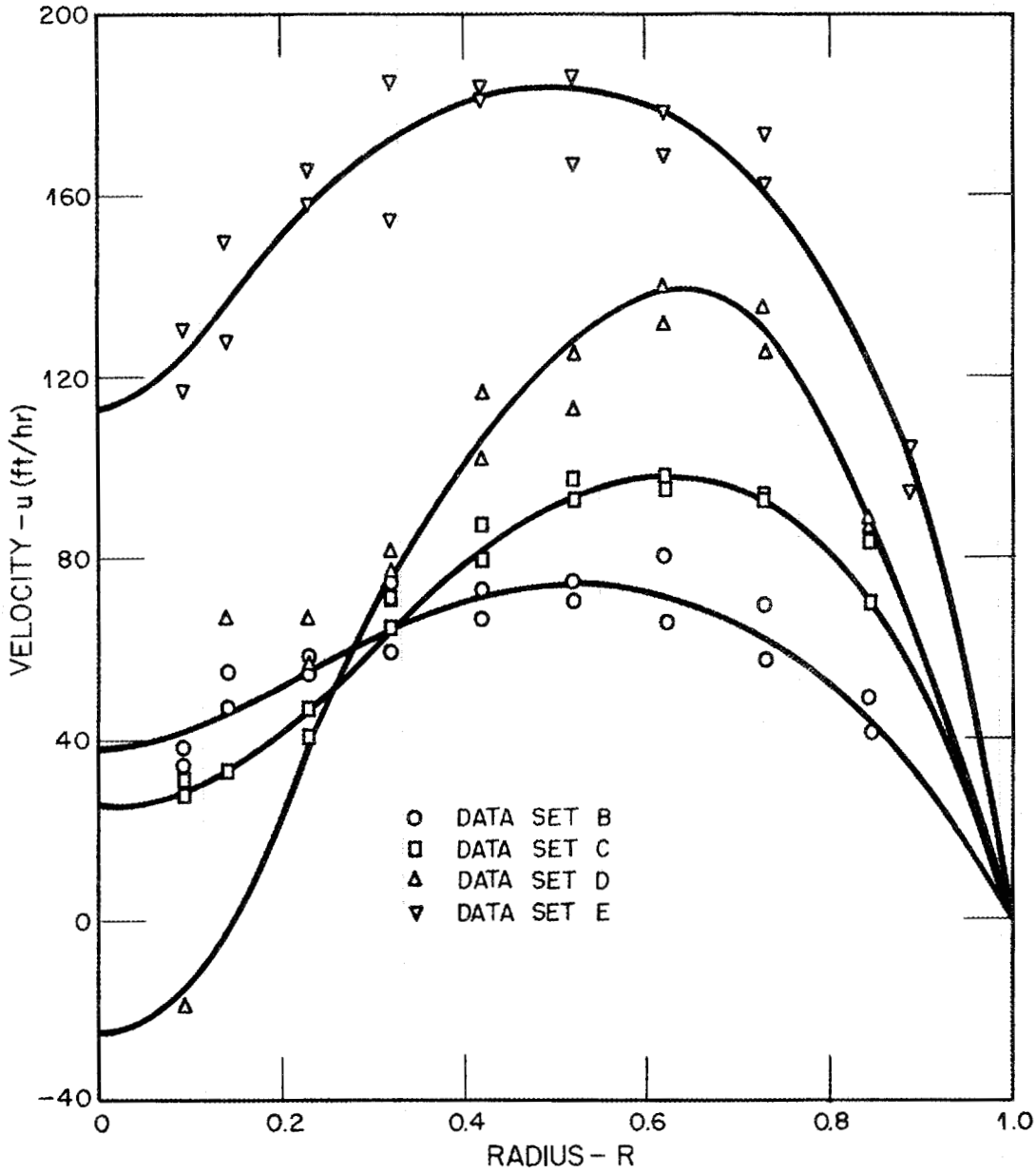

Fig. 6. Velocity Profile in the Cold Leg of a Thermal Convection Harp at $X = 0.677$ $\left(\frac{y}{d} = 20\right)$

especially true for the case of Data Set D. By coincidence, the transition from laminar to turbulent boundary layer occurred for Data Set D at the position of observation. Thus, the flow in the center of the pipe was unstable, being sometimes laminar and sometimes turbulent. That is the reason for the scatter in these data for Data Set D. In view of this it would have been permissible, perhaps, to draw two profiles for Data Set D. The velocity profile for Data Set E is obviously turbulent. Although velocity observations were not made in the horizontal or transverse sections of the harp one would expect the flow through these sections to be that characteristic of the forced flow associated with the value of the Reynolds modulus. All the Reynolds moduli in this experiment are well below the critical Reynolds modulus for isothermal forced flow. Therefore one would expect the turbulence that was initiated in the cold or hot vertical legs to be quickly damped out in going through the horizontal legs. The fact that the turbulence observed near the entrance to the top of the cold leg was minimum supports this belief.

The Temperature Structure

The wall temperatures were measured at various locations in the hot and cold legs. The wall temperature data for the conditions of Data Set C are plotted in Figure 7. In Figure 8 curves are shown which indicate the extremes of the form of the wall temperature data for the various experiments. At the lower values of the Grashof modulus the wall temperatures more nearly approached a square wave distribution; that is, $\Phi_W = 0$ for the cold leg and $\Phi_W = 1$ for the hot leg. In Figures 9 and 10 the fluid temperature profiles predicted and

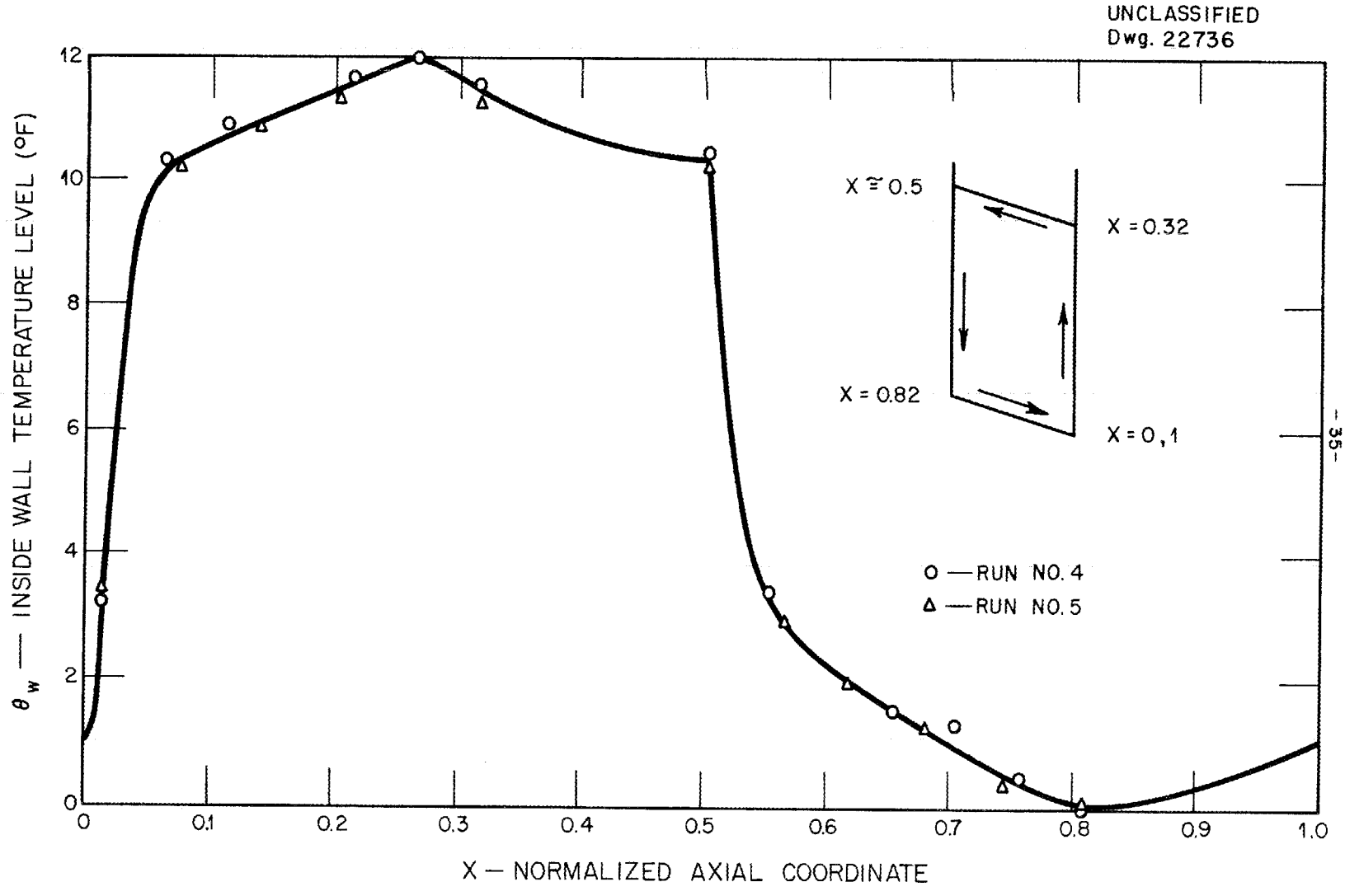

Fig. 7. Inside Wall Temperatures for Thermal Convection Harp (For the Conditions of Data Set C)

UNCLASSIFIED
Dwg. 22737

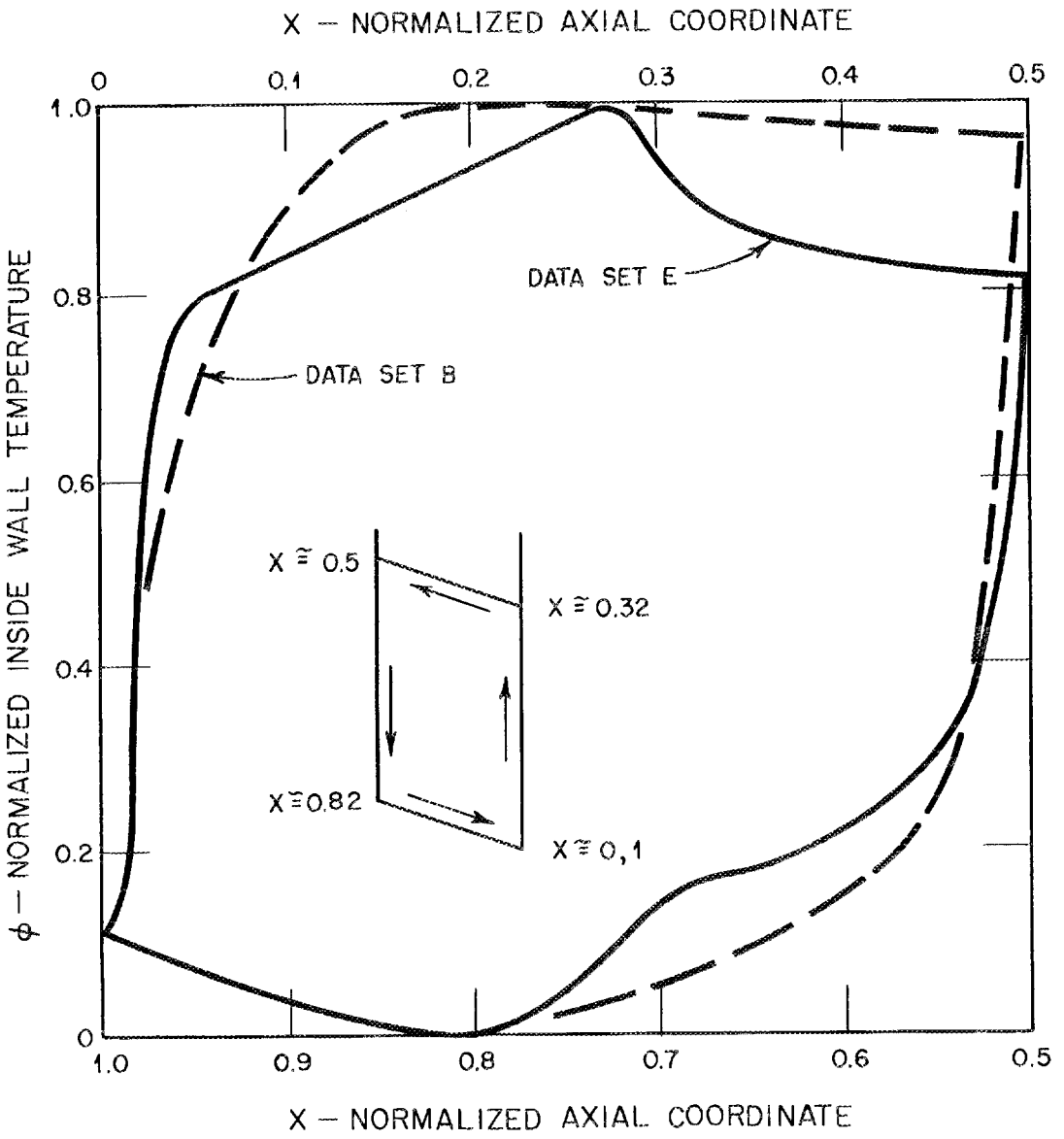

Fig. 8. Form of Wall Temperature Distribution Curves for the Present Work.

UNCLASSIFIED
Dwg. 22738

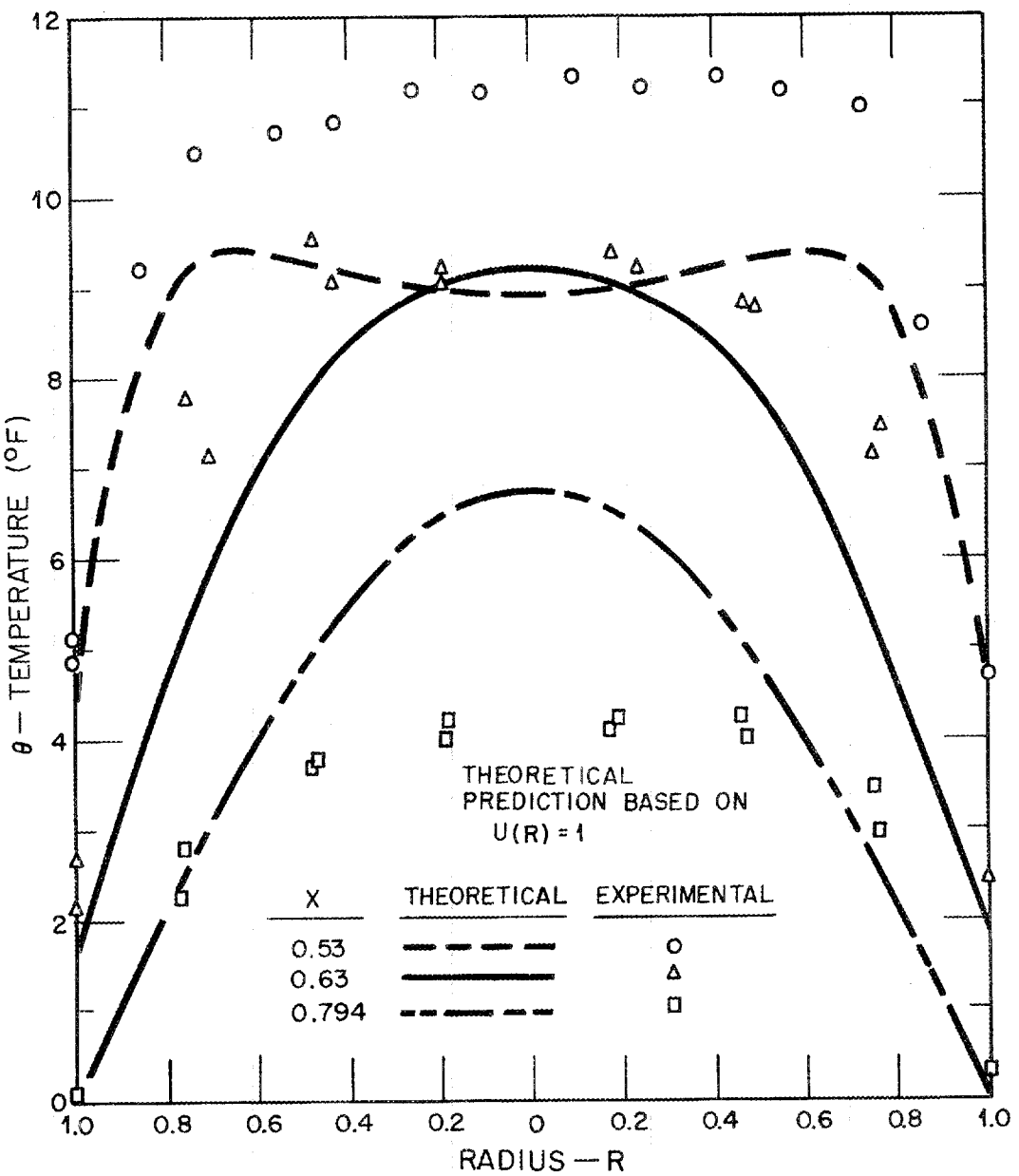

Fig. 9. Comparison of Predicted and Measured Fluid Temperatures in the Cold Leg of a Thermal Convection Harp (For the Conditions of Data Set C)

UNCLASSIFIED
Dwg. 22739

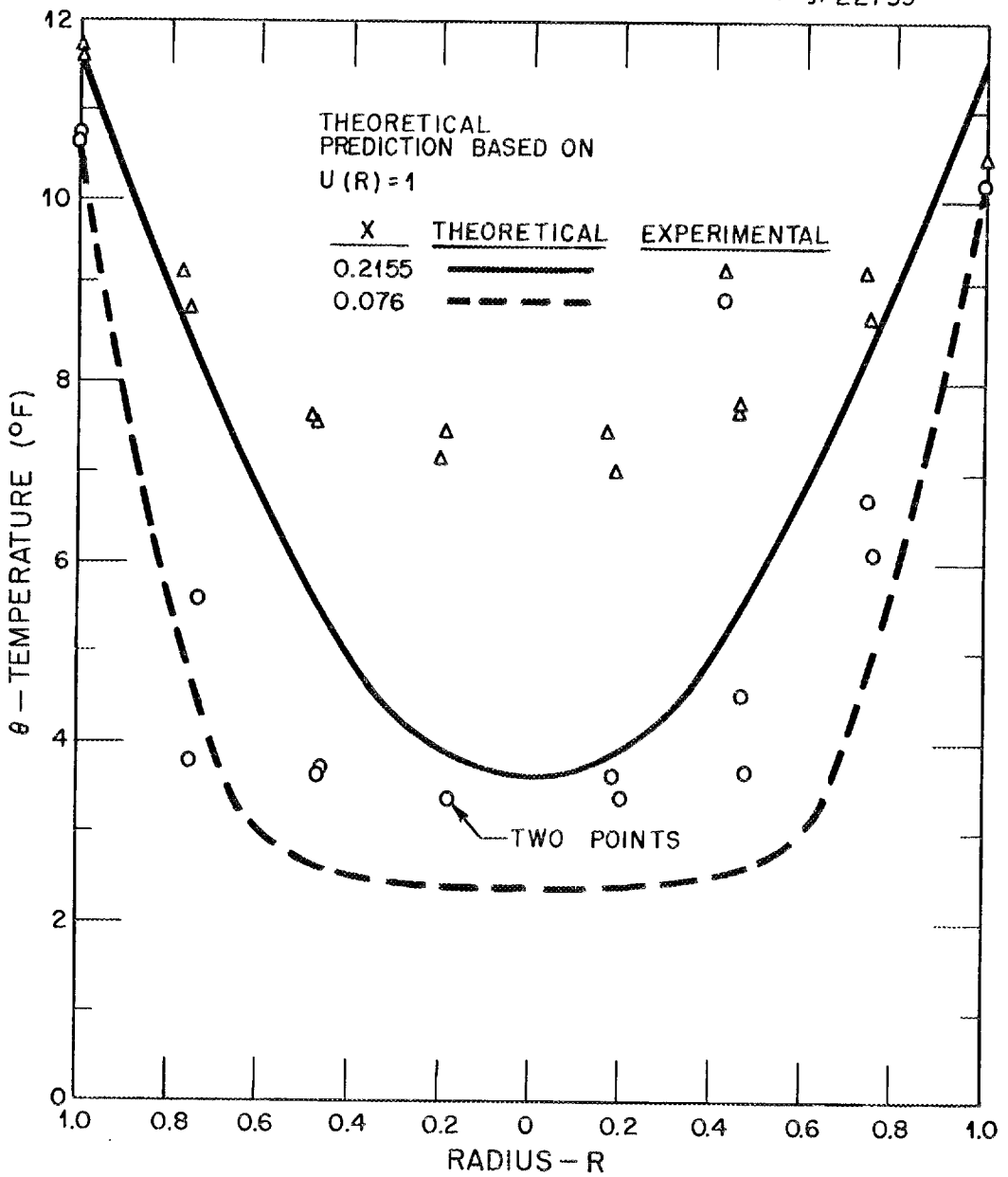

Fig. 10. Comparison of Predicted and Measured Fluid Temperatures in the Hot Leg of a Thermal Convection Harp (For the Conditions of Data Set C)

TABLE II

VALUES OF $\Delta\Phi_b$, NORMALIZED BUOYANT TEMPERATURE DIFFERENCE, AS COMPUTED FROM THE NUMERICAL SOLUTION OF THE CONVECTION EQUATION FOR LAMINAR FLOW

Postulated Velocity Distribution	Form of Wall Temperature Distribution	Postulated Value for Graetz Modulus		
		8	16	32
U = 1	Data Set B	0.152	0.103	0.076
	Data Set C	0.158	0.108	0.080
	Data Set D	0.159	0.103	0.076
	Data Set E	0.144	0.099	0.073
	Square Wave*	-----	0.245	0.179
U = 6R(1-R)	Data Set B	0.164	0.135	0.114
	Data Set C	0.166	0.138	0.116
	Data Set D	0.158	0.132	0.111
	Data Set E	0.153	0.127	0.107
	Square Wave*	0.336	0.266	0.215

*Square Wave indicates $\Phi_w = 1$ for $0 < X < 0.5$ and $\Phi_w = 0$ for $0.5 < X < 1$

measured are compared. The presence of turbulence caused the transport of heat within the fluid to be greater than that predicted by the laminar flow solution. Temperature profiles for these same axial locations were also taken for the case of Data Set E. The degree of turbulence was even greater and the agreement between the predicted and the measured fluid temperatures was not as good. For this reason the curves for this case are not shown.

The normalized buoyant temperature differences computed from the numerical analysis are tabulated in Table II. The decision to perform an experiment for the conditions of Data Set A was made after the machine calculations had been completed. The normalized wall temperature data for Data Sets A and B were very similar. From Table II it can be observed that the computed values of $\Delta\Phi_b$ for Data Sets B, C, and D are almost identical. On the basis of these two observations it was decided to use the $\Delta\Phi_b$ values computed for Data Set B in predicting the Reynolds modulus for Data Set A. The "square wave" calculation corresponds to the limiting value of the wall temperature distributions for these experiments.

Evidences of Turbulence

A description of the visual observations of the transition to turbulent flow was given earlier. In Table III may be seen the amplitude and frequency of the fluctuations in fluid temperature at five axial positions in the harp. The minimum values occurred at the wall and the maximum values occurred at a location between the wall and the center of the tube. Although it was not possible to obtain quantitative data on the intensity of turbulence in the case

TABLE III

COMPARISON OF TURBULENT INTENSITY FOR DATA SETS C AND E AS DERIVED FROM THE FLUID TEMPERATURE TRAVERSES

Axial Location	Range of Amplitude of Temperature Oscillation - °F		Range of Average Frequency of Temperature Oscillation - Cycles per min.	
	Data Set C	Data Set E	Data Set C	Data Set E
X = 0.076	0	0 to 1	0	0 to 14
X = 0.216	0 to 2.5	3 to 9	0 to 14	22 to 65
X = 0.528	0	0 to 2	0	1.5 to 12
X = 0.629	0	0.5 to 8	0	3 to 40
X = 0.794	0 to 1.5	2 to 8	0 to 15	15 to 45

of the visual observations of the droplets, the qualitative observations do not disagree with the data in Table III.

It is interesting here to contemplate what the equivalent friction factor, λ, might have been for these experiments. It is recalled that for the cases of Data Sets C and E the temperature profiles in fluid were measured at five different positions within the harp. From these data five values of the mean temperature can be computed, and from these five mean temperatures the buoyant temperature difference can be determined. Within the accuracy of this procedure the resulting buoyant temperature difference is that actually existing in the fluid and is not a computed one. Since the actual temperature curves were very similar to those computed by the numerical analysis, one can establish fairly accurately the mean temperature curve on the basis of only five mean temperatures. It is recalled that, earlier, the dynamic equation for a thermal convection harp was derived as:

$$Re = \left(\frac{2}{\lambda}\,\frac{h_o}{L}\,Gr_d\,\Delta\Phi_b\right)^{1/2} \quad \ldots\ldots\ldots\ldots \quad (4)$$

$$K_\lambda = \frac{\lambda}{\lambda_{lam.}} = \frac{\lambda\,Re}{64} \quad \ldots\ldots\ldots\ldots \quad (19)$$

$$K_\Phi = \frac{\Delta\Phi_b}{(\Delta\Phi_b)_{cal.}} \quad \ldots\ldots\ldots\ldots \quad (20)$$

For the two Data Sets, C and E, now being discussed, all parameters in Equation (4) have been determined by measurements in the experiment except the friction factor, λ, which can then be computed. The two values of friction

factor thus determined are indicated in Figure 11 as measured values of λ. In Equations (17) and (18) the factors K_λ and K_Φ are defined. For the isothermal laminar flow in a long, straight pipe of circular cross section, the value of K_λ is equal to unity. The effect of elbows, bends or turbulence will tend to increase the value of K_λ. A value for K_Φ equal to unity indicates that the computed value of $\Delta\Phi_b$ is accurate. It is interesting to note here that the calculated value of $\Delta\Phi_b$ may be quite accurate even for the case where the temperatures from which it was computed are in rather great error. It is recalled that in Equation (15b) the value of $\Delta\Phi_b$ calculated was computed from a postulated value of Reynolds modulus. It will be assumed here that the value of K_Φ is equal to unity when the $\Delta\Phi_b$ calculated is based on the experimentally determined Reynolds modulus. Putting (17) and (18) in (4) get:

$$Re = \frac{K_\Phi}{K_\lambda} \frac{1}{32} \frac{h_o}{L} Gr_d \, (\Delta\Phi_b)_{cal.} \quad \ldots\ldots\ldots\ldots \quad (8b)$$

On the basis of the postulate that K_Φ is equal to unity (8b) is reduced to (8c).

$$(K_\lambda \, Re)_{cal.} = \frac{1}{32} \frac{h_o}{L} Gr_d \, (\Delta\Phi_b)_{cal.} \quad \ldots\ldots\ldots \quad (8c)$$

$$\frac{(K_\lambda \, Re)_{cal.}}{(Re)_{meas.}} = K_\lambda \quad \ldots\ldots\ldots\ldots\ldots \quad (19)$$

Now it is necessary to refer to Figure 2, where the graphical solution was obtained for the conditions of Data Set C. From Equation (8c) it is seen that, for a postulated Reynolds modulus equal to that which was measured in the experiment, the value of the ordinate is equal to the product K_λ times Reynolds modulus. Putting this in Equation (19), one can compute the value of K_λ; from

UNCLASSIFIED
Dwg. 22740

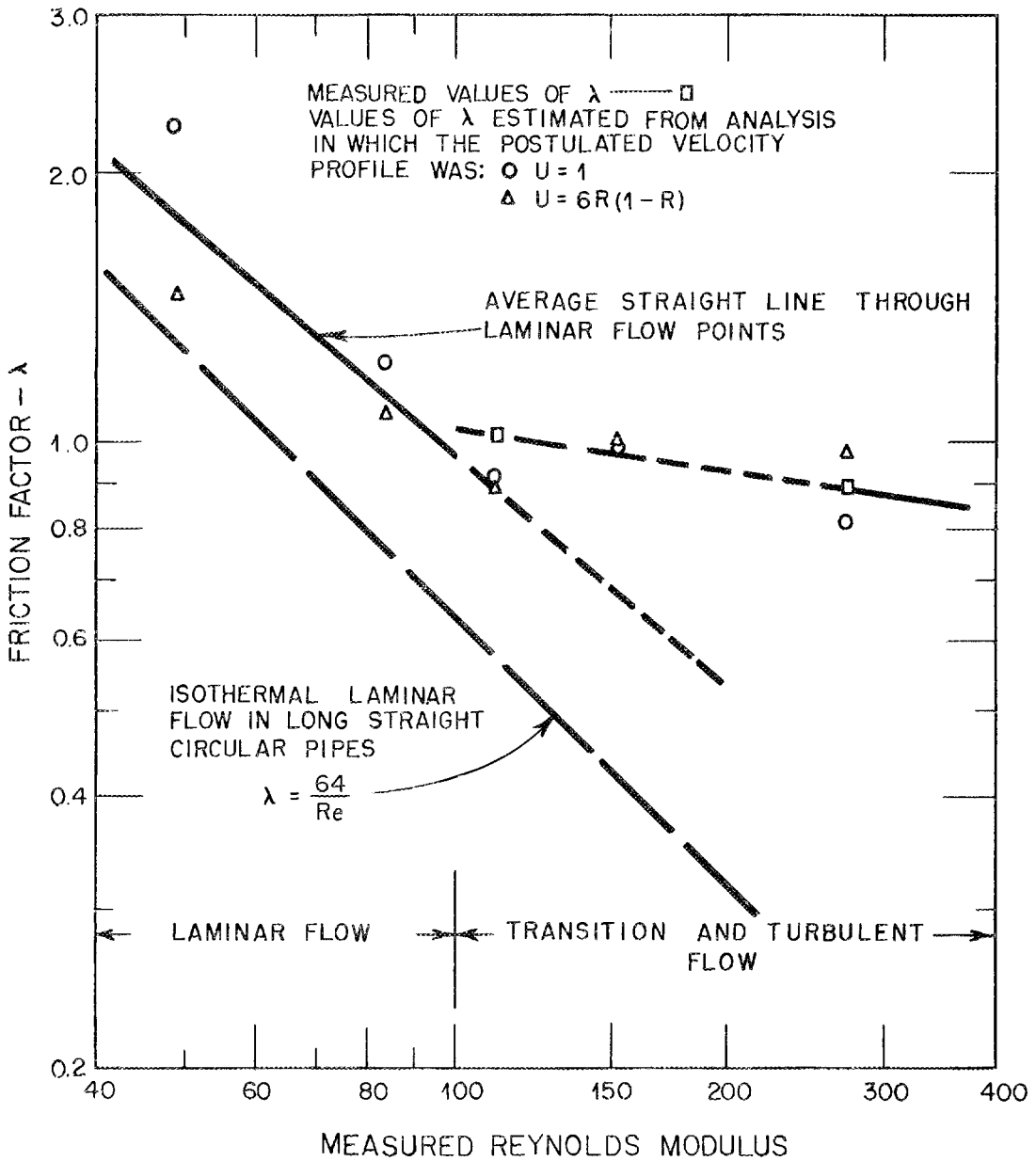

Fig. 11. Measured and Estimated Friction Factors for Thermal Convection Harp.

the value of K_λ and Re, one can compute the value of λ. A numerical example based on Figure 2 may be helpful here. It is recalled that the Reynolds modulus measured in the experiment based on the conditions of Data Sets C was 111. From Figure 2 the values of the ordinate for a value of the abscissa equal to 111 are 170 and 174 respectively. From this, one computes values of K_λ to be 1.53 and 1.565 respectively; the corresponding values for λ are 0.882 and 0.902, respectively. This procedure was used to obtain each of the values of estimated friction factors given in Figure 11. There are two interesting observations concerning Figure 11. The first is the striking similarity between Figure 11 and a similar plot for the isothermal forced flow of a fluid through a system having several bends. A significant difference in the two cases is the value of Reynolds modulus at which transition to turbulence occurs; for the harp this value was 110, while for the forced flow system it would be about 20 times greater, or 2200. The second interesting observation is the good agreement between the two different methods which were used for the cases of Data Sets C and E. Figure 11 is presented as a matter of interest, not for use as a source for quantitative information concerning friction factors. One could determine the friction factor in a harp rather accurately from measurements of fluid temperature and mean velocity. However the number of temperature data necessary would be much greater than was obtained here.

In correlations of heat transfer, friction, mass transfer and similar phenomena the transition from laminar flow to turbulent flow is usually easily recognized by an abrupt change in the slope of the curve. It is interesting to note that in Figure 12 the indication of a change in flow regime agrees with the other observations previously discussed.

UNCLASSIFIED
Dwg. 22741

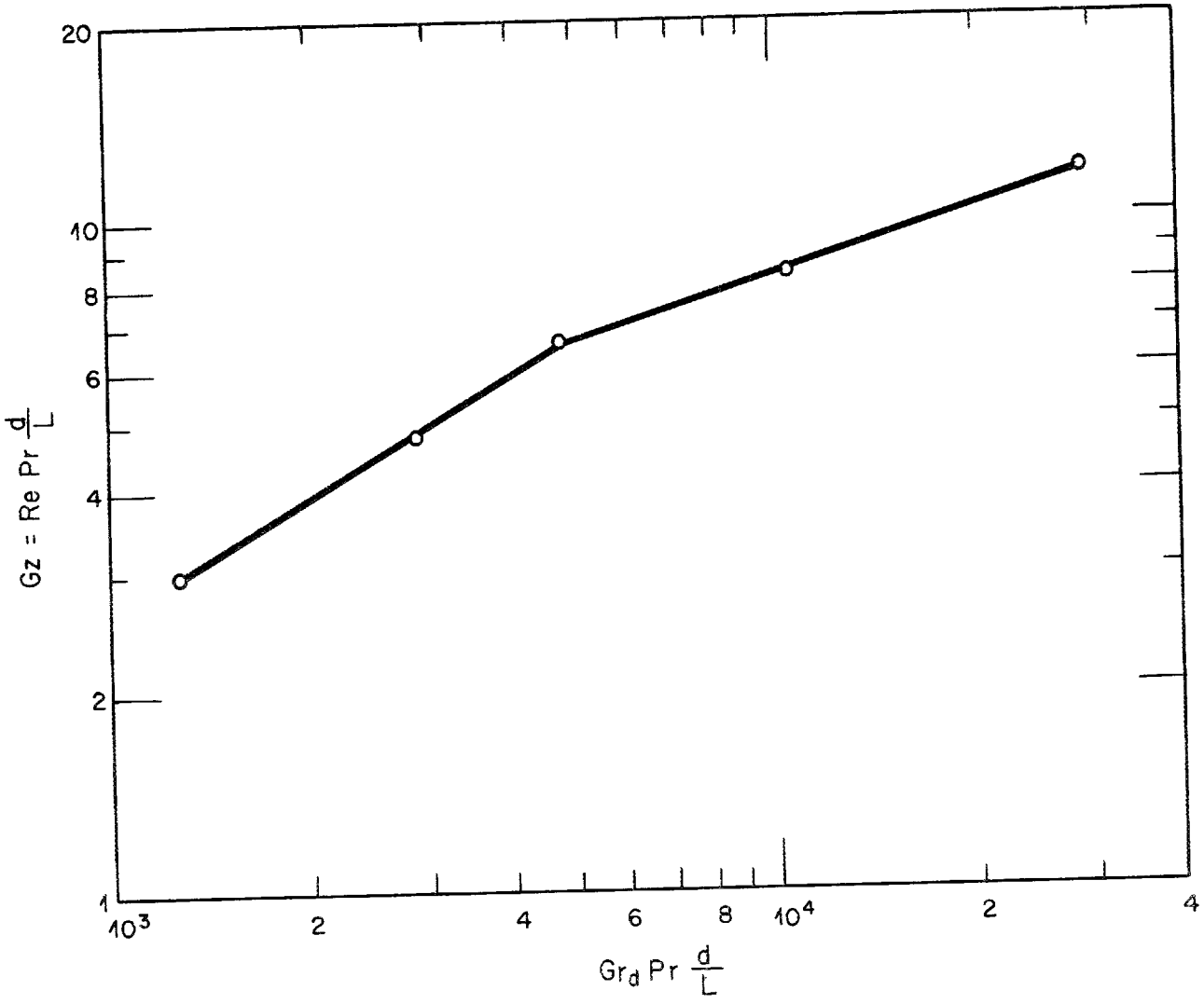

Fig. 12. Graetz Modulus Versus Grashof Modulus Times Prandtl Modulus Times d/L for a Thermal Convection Harp.

Comparison of Measured and Predicted Reynolds Moduli

The predicted value of Reynolds modulus is plotted in Figure 13 versus the measured value. It is recalled that, for these predictions, the friction factor was postulated to be the same as that for isothermal laminar flow in a long, straight pipe of circular cross section. The non-isothermal velocity profile and the bends in the harp would cause the effective friction factor to be greater than the postulated one; consequently, the resulting predictions would always be too high. The velocity profile was observed to vary with axial position; for the computation of the thermal structure the velocity profile was postulated to be constant. From Figure 13 it is seen that the correlation is better than 30% in the range of Reynolds moduli where the flow was laminar. For values of Reynolds modulus greater than 100, where the flow was observed to be turbulent in part of the circuit, the prediction was not good.

The ideal system or thought model employed in the development of the equations used to predict the Reynolds modulus was a forced flow model. In the discussion of the experimental results the authors have emphasized the free flow nature of the dynamic structure. It was previously stated that the flow is described more accurately as both free and forced or superimposed-free-and-forced-flow. Martinelli and co-workers in references 4 and 5 derived Equation (20) which satisfactorily correlated a vast quantity of heat transfer data for the case of superimposed-free-and-forced laminar flow convection in a vertical pipe of circular cross section and having a uniform wall temperature.

UNCLASSIFIED
Dwg. 22742

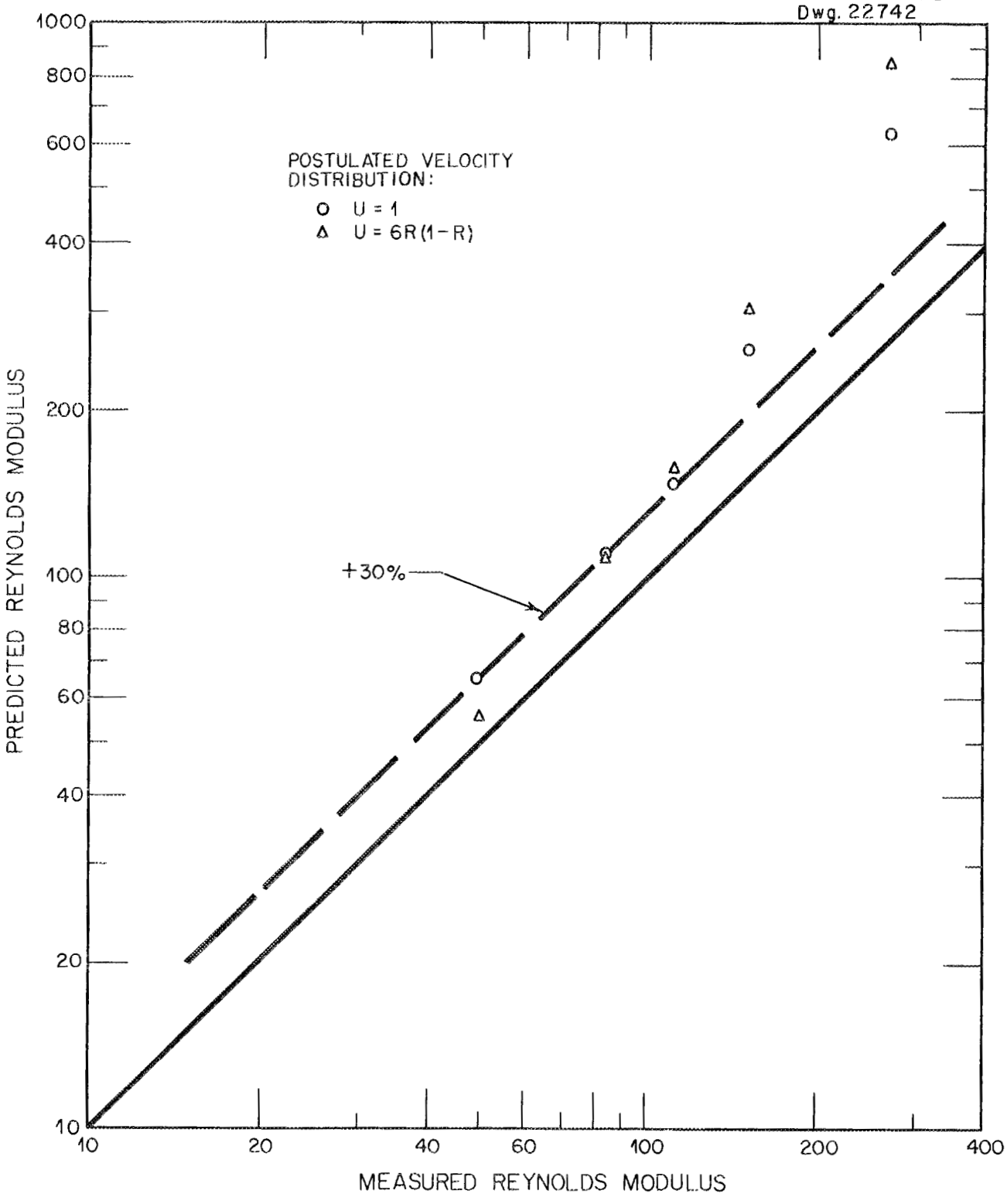

Fig. 13. Comparison of Predicted Reynolds Modulus and Measured Reynolds Modulus.

$$Nu = 1.75\ F_1 \left(\frac{\pi}{4}\ Gz + 0.0722\ F_2 (Gr_d\ Pr\ \frac{d}{L})^{3/4}\right)^{1/3} \quad \ldots . \quad (20)^*$$

The wall temperatures in Data Sets A and B approximated this condition in each of the vertical legs. One might use Equation (20) to classify laminar flow convection as forced, free, or mixed flow, depending on the influence that neglecting one of the terms would have on the Nusselt modulus. Eckert, et. al., in reference 6, have suggested such a classification for the case of very short tubes (L/d = 5). For the conditions of Data Set B the Nusselt modulus as computed in Equation (20) is 16% lower when the forced flow influence is neglected than when both are considered. It would seem that the superimposed-free-and-forced-flow in the vertical legs of a thermal convection harp is more characteristic of free flow than of forced flow for two reasons; first, the success with which the growth and transition of the boundary layer was described by a free convection model; second, the fact that the forced flow component contributed only 16% to the Nusselt modulus as computed from Equation (20).

---

*The factors F_1 and F_2 in Equation (20) are not constants. The user should consult the original reference where the complicated variation of these factors with Nu and Gz is given.

CONCLUSIONS

Experiments were performed for the free flow of water in a 0.7 inch I.D. Pyrex thermal convection harp having an effective height of 2.5 feet. The experiments were conducted for five different sets of conditions corresponding to ranges of Grashof moduli and Reynolds moduli of 2×10^4 to 70×10^4 and 50 to 270, respectively. Velocity measurements were made in the cold leg of the harp; wall temperature and fluid temperature traverses were made in both legs. A method was proposed for predicting the Reynolds modulus from wall temperature data by means of a numerical solution of the laminar flow heat conduction equation. On the basis of these investigations the following conclusions are submitted:

1) In any forced flow where a radial temperature difference exists there is a superimposed free convection effect, and, depending on the relative magnitudes of the Reynolds modulus and the Grashof modulus, the two phenomena may be of equal importance or one may be negligible. The forced flow influence seems to be of secondary importance for the flow of ordinary fluids in the vertical legs of a thermal convection harp for two reasons; first, free convection equations satisfactorily predicted the growth and transition of the boundary layer in the cold leg; second, the forced flow component contributed only 16% to the Nusselt modulus as computed from the Martinelli equation for superimposed free and forced viscous convection in

a vertical pipe. It follows that the heat transfer and mass transfer is predicted by free convection, not forced convection correlations, unless both influences are considered.

2) For values of the Reynolds modulus greater than 100 the Grashof modulus was large enough to cause approximately half of the hot and cold legs to be in turbulent flow. Thus, the laminar flow regime for this harp must be considered to be below a Reynolds modulus of 100 rather than around 2000, the familiar value for isothermal forced flow.

3) The predicted values of the Reynolds modulus were consistently greater than the measured values. In the range of Reynolds moduli below 100, where the flow was essentially laminar, the correlation was better than 30%. In the turbulent regime the method is not applicable.

4) The nature of the flow in a thermal convection harp is greatly influenced by two factors: the properties of the fluid and the manner in which heat is added and removed. The wide spectrum over which each of these factors may vary makes it impossible to perform a general analysis that is applicable to all cases. This work was done for a fluid having a moderate value of kinematic viscosity;

transitional flow was observed. One would expect to obtain highly turbulent flow for fluids of low viscosity such as liquid metals and definitely laminar flow for highly viscous fluids.

REFERENCES

1. Hackett, H. N.: Mercury for the Generation of Light Heat and Power, ASME Tr., October 1942, Vol. 64, p. 647.

2. Goldstein, S.: Modern Developments in Fluid Dynamics, Vol. II, p. 642, Oxford Press, 1938.

3. Eckert, E.R.G. and Soehngen, E.: Interferometric Studies on the Stability and Transition to Turbulence of a Free-Convection Boundary Layer, Proceedings of the General Discussions on Heat-Transfer, 1951, p. 321. Sponsored by IME and ASME.

4. Martinelli, R. C., Southwell, C. J., Alves, G., Craig, H. L., Weinberg, E. B., Lansing, N. F., and Boelter, L.M.K.: Heat Transfer and Pressure Drop for a Fluid Flowing in the Viscous Region through a Vertical Pipe, A.I.Ch.E. Tr., Vol. 38, 1942, p. 493.

5. Martinelli, R. C. and Boelter, L.M.K.: The Analytical Prediction of Superimposed Free and Forced Viscous Convection in a Vertical Pipe, University of California Publications in Engineering, Vol. 5, 1942.

6. Eckert, E.R.G., Diagnila, A. J., and Curren, A. N.: Experiments on Mixed-Free-and-Forced-Convective Heat Transfer Connected with Turbulent Flow through a Short Tube, NACA T.N. 2974, July, 1953.

APPENDIX

Apparatus and Procedure

The design of the harp was begun with the premise that the velocity measurements would be made by the visual observation of suspended droplets in the primary fluid. This made it necessary that the walls be transparent and it essentially dictated the method of heat addition and removal that was used. During the course of the experiment a concerted effort was expended toward minimizing the cost of the apparatus by using only those materials and instruments that were on hand.

Harp arrangement

The primary flow circuit of the harp consisted of 0.695 inch I.D. Pyrex tubing with an effective height of 30.4 inches and a centerline length around the loop of 78.9 inches. The hot leg extension, as shown in Figure 14, was installed to provide access to the hot leg for wall and fluid temperature thermocouple probes; this extension was insulated to reduce heat loss to the air. A similar means of access was provided for the top of the cold leg. Each of the four legs was provided with a heat exchanger by the attachment of 1.2 inch I.D. Pyrex tubes over the length of the legs. The exchangers on the upper and lower connecting legs were never used as heat exchangers; however they did serve to somewhat insulate these legs from the air and reduce heat losses. Heat was removed from the cold leg by circulating cold water from the building supply through the cold leg exchanger. Three needle valves on the hot leg exchanger inlet line permitted the building hot and cold water to be mixed to obtain the desired hot leg exchanger inlet temperature. Thermocouple wells were installed to permit measurement of inlet and outlet exchanger temperatures.

UNCLASSIFIED
Dwg. 22743

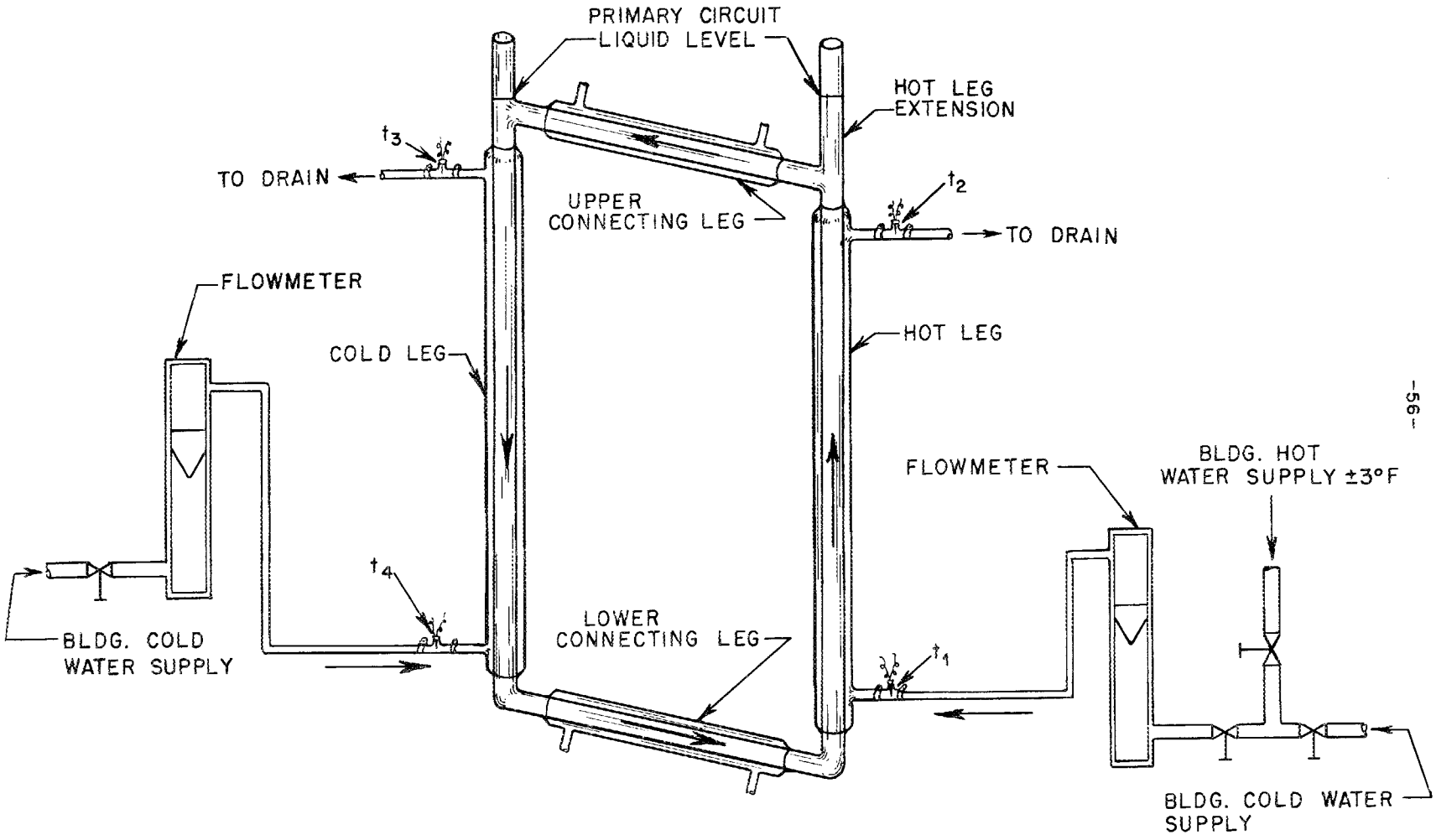

Fig. 14. Schematic Sketch of Primary and Secondary Circuits for Thermal Convection Harp Experiment.

The secondary flow was measured by rotometers. The flow rate to each exchanger was maintained at one gallon per minute for all experiments performed. In order to stabilize the flow in the upper and lower connecting legs these legs were inclined from the horizontal orientation and the hot and cold legs were chosen so that the flow from the hot leg to the cold leg would have an upward component. In Figure 15 the box enclosing the optical arrangement for velocity measurements is shown attached to the cold leg.

Instrumentation for velocity measurements

The velocity profiles were measured by timing the trajectory of oil droplets viewed in their scattered light. The time for a droplet to traverse the distance between two horizontal marks separated by a vertical distance of one inch was measured with a stop watch; simultaneously, by reference to vertical alignment marks, the radial position of the droplet was observed. The plan view of the arrangement for the vertical alignment marks is shown in Figure 16.

From the results of a refraction analysis four alignment marks were scratched on the front and rear plastic plates shown in Figure 16; when the plates were properly aligned, the line of sight cut through the test section at radii of $\pm$ 0.2 and $\pm$ 0.6 along a radius perpendicular to the line of sight. A similar set of plates were used to align the light beam. The alignment of the front and rear plates was accomplished with the aid of a third plate that was inserted in the primary system during alignment. A sealed beam spotlight was used as the light source; the light was collimated with a slit system so that it illuminated a zone of the test section 0.2 d in width at the center of the tube. The plastic box enclosure prevented condensation on the cold exchanger

UNCLASSIFIED
PHOTO 20400

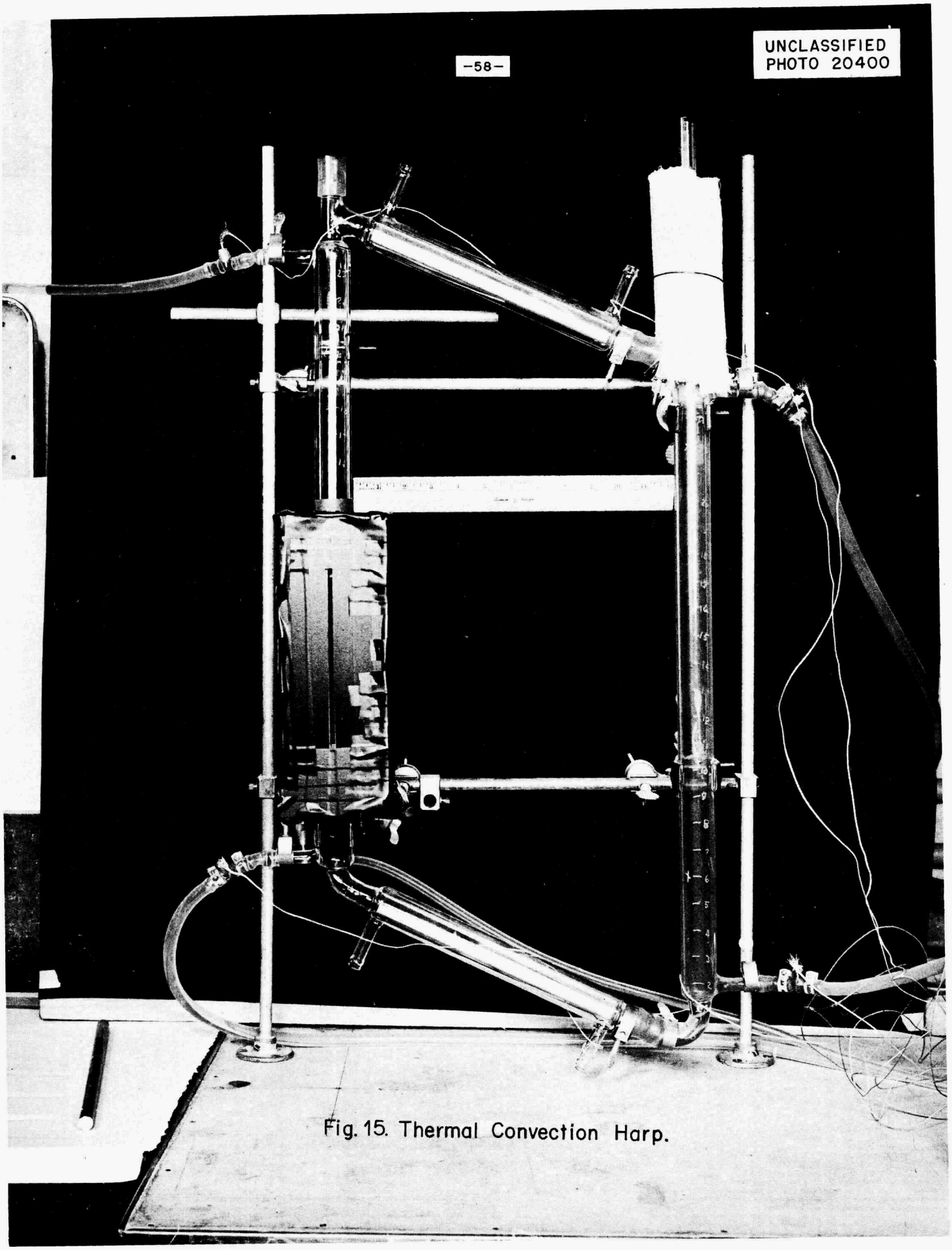

Fig. 15. Thermal Convection Harp.

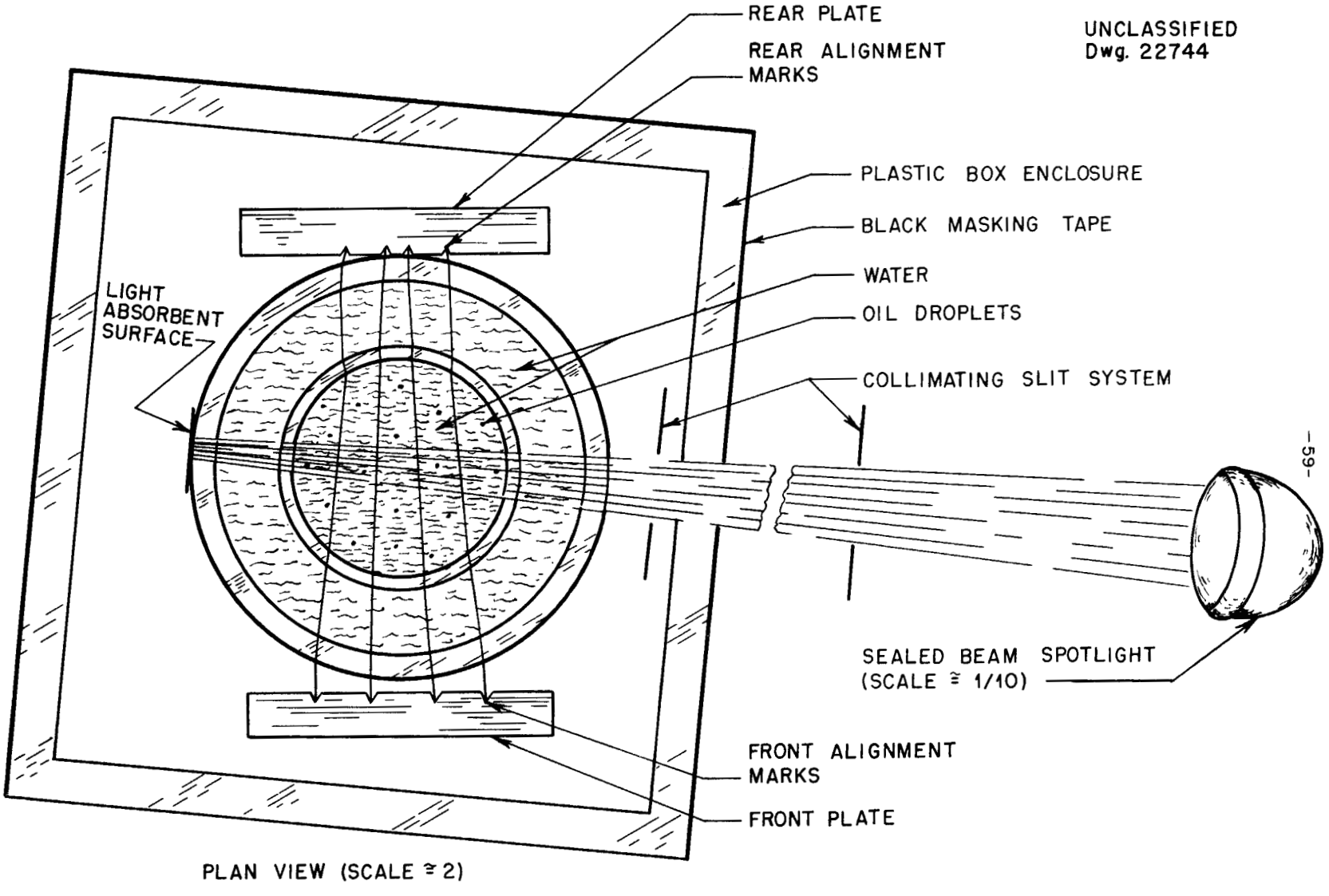

Fig. 16. Optical Arrangement Used in Measuring Particle Velocities (Plan View)

wall; black masking tape on three sides of the box served to reduce the random light from the laboratory. The scattered light intensity from the droplets was insufficient at an angle of 90° to the beam. Satisfactory intensity was available at 85°, so the observations were made at that angle. The scattered light was intense at an angle of about 135°; this is the angle at which the qualitative observations were made. In Figure 15 the view is in the direction of the light beam and the second collimating slit may be seen. The observer viewed the apparatus from the left of the photograph.

Instrumentation for temperature measurements

The thermocouple probe used for measuring the internal wall temperature is shown in Figure 17. The spring action of the two pieces of piano wire caused the thermocouple wires to be pressed against the Pyrex pipe wall for approximately 0.5 inches above and below the thermocouple junction. This served to reduce the error due to conduction along the wires.

The thermocouple probe in Figure 18 was used to measure the fluid temperatures. The thermocouple wires used here were 0.003 inches in diameter and were coated with a 0.001 inch layer of Teflon. The thermocouple-leads were brought up through a three foot length of thermocouple-lead tubing. The thermocouple-lead tubing was held in place by a two inch long guide tube. Piano wire springs kept the guide tube against the wall of the Pyrex tubing. Small shoulders on the thermocouple-lead tubing at each end of the guide tube served as thrust bearings; this permitted rotation and prevented axial translation of the thermocouple lead-tubing relative to the guide tube. The thermocouple-lead tubing extended two inches below the guide tube; at this point the thermocouple leads emerged and extended radially to the center of the pipe. A pointer and protractor

UNCLASSIFIED
Dwg. 22745

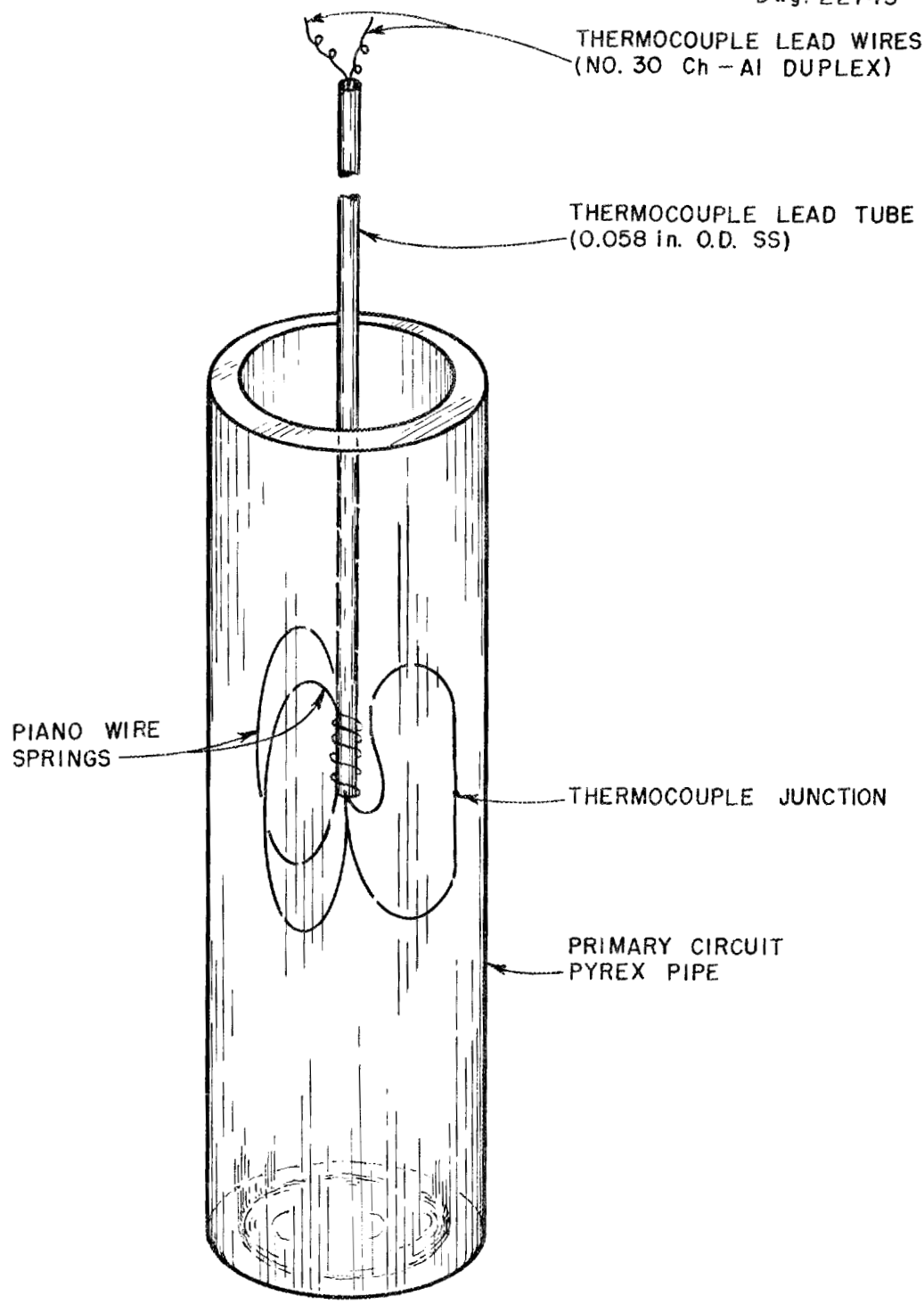

Fig. 17. Wall Temperature Thermocouple Probe

UNCLASSIFIED
Dwg. 22746

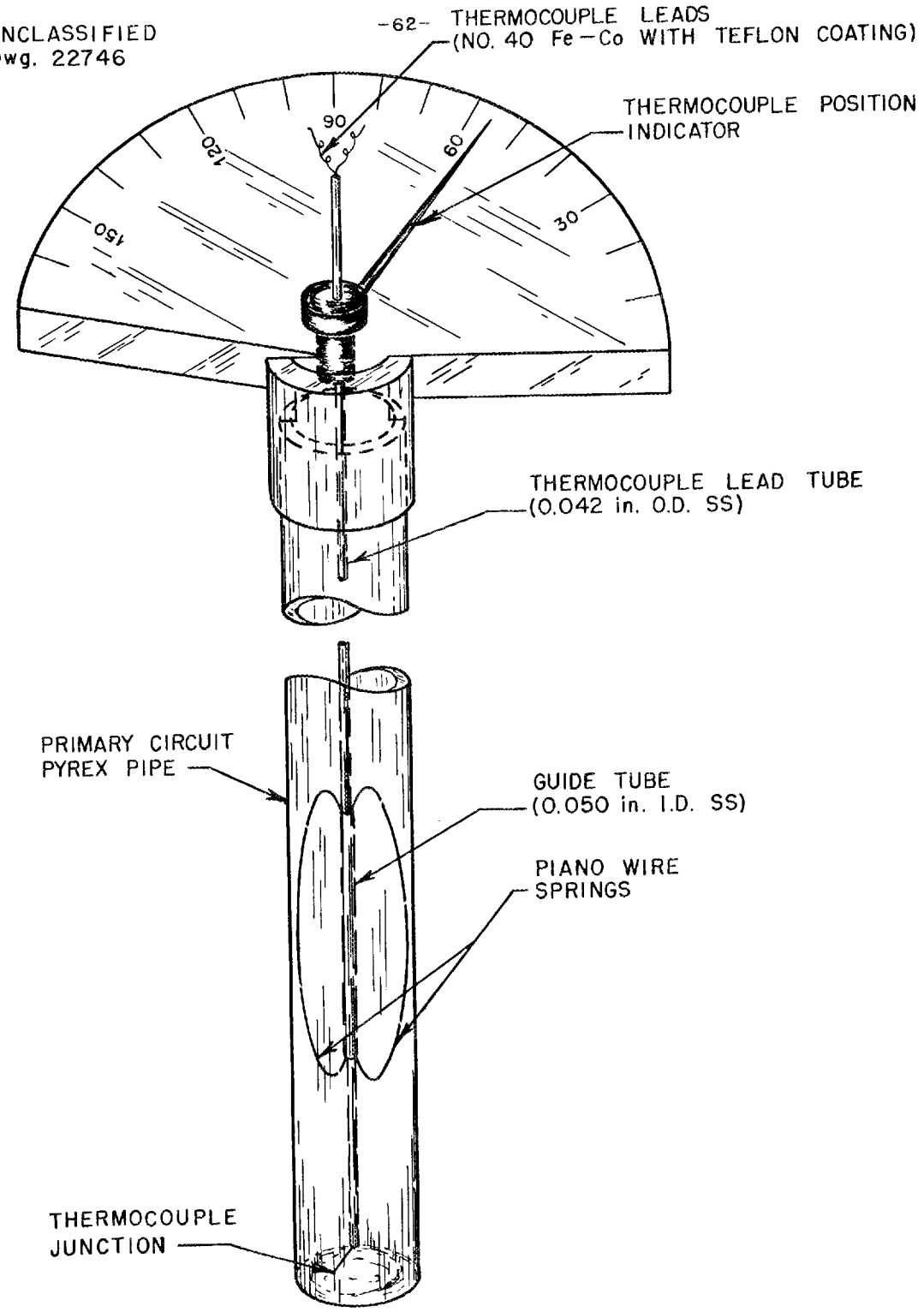

Fig. 18. Fluid Temperature Thermocouple Probe.

arrangement at the top of the hot or cold leg extension was used to control and to indicate the angle of rotation of the thermocouple junction. When the assembly had been positioned at the desired axial location the thermocouple was rotated until the junction touched one wall of the pipe. The uncertainty in locating the position of the pipe wall was less than two degrees of arc; this corresponded to an error in radius of less than two percent. The fluid temperature profiles could then be measured by this device at various axial positions in the hot and cold legs.

When the voltage response from the thermocouples was steady the measurement was made with a Leeds and Northrup Portable Precision Potentiometer. In the turbulent regions, when the temperature was fluctuating, the thermocouple voltage was recorded on a Brown strip recorder.

Experimental procedure

The flow in the primary circuit of the harp was set and maintained by controlling the inlet temperatures of the two heat exchangers that comprised the secondary circuit. The flow rate through each exchanger was maintained at one gallon per minute for each of the experiments. Since the cold water temperature remained essentially uniform throughout a given run the factor that was set and controlled was the difference between the hot and cold exchanger inlet temperatures. For Data Sets B, C, D, and E the value of this temperature difference was 7.5, 15, 30, and 60 degrees F., respectively. The maximum variation in this temperature difference for all runs comprising a Data Set was five percent.

The velocity runs usually required six hours; one hour for the system to reach steady state and get the optimum distribution of droplets, four hours to make the 200 to 250 velocity observations, and one hour to measure the wall

temperatures in the hot and cold legs. The Meriam Unity Oil droplets used in these observations were of the order of 0.01 inches in diameter. The velocity observations were all made in that half of the cold leg near the entrance of the light because the intensity of the light scattered from the droplets in the other half was too low to permit satisfactory observations. No velocity observations were made in the hot leg because the rust deposit on the walls of the hot leg exchanger reduced the visibility rather greatly. With the aid of the four visual alignment lines and the two formed by the walls of the test section the droplets were observed to be in one of the ten radial compartments as shown in Figure 19. The timing was done with a stop watch having a sweep second hand. The smallest division on the watch was 0.02 seconds; it can thus be safely assumed that the error in measuring the time was due entirely to the observer's limitations.

Treatment of Velocity Data

The analysis of the velocity data would have been simplified if a beam of width equal to 0.02 d could have been used instead of the value of 0.2 d that was used. With the former value of beam width the variation of the radius in a given compartment could have been considered negligible for the purposes of this work. Due to the turbulence, the droplets sometimes had relatively high velocity components in the radial and angular directions. If the observations had been made in a shorter time, and therefore for a shorter distance, or if the flow had been laminar throughout the experiment the smaller beam width could have been used. A timing distance of one inch was chosen as the optimum length

UNCLASSIFIED
Dwg. 22747

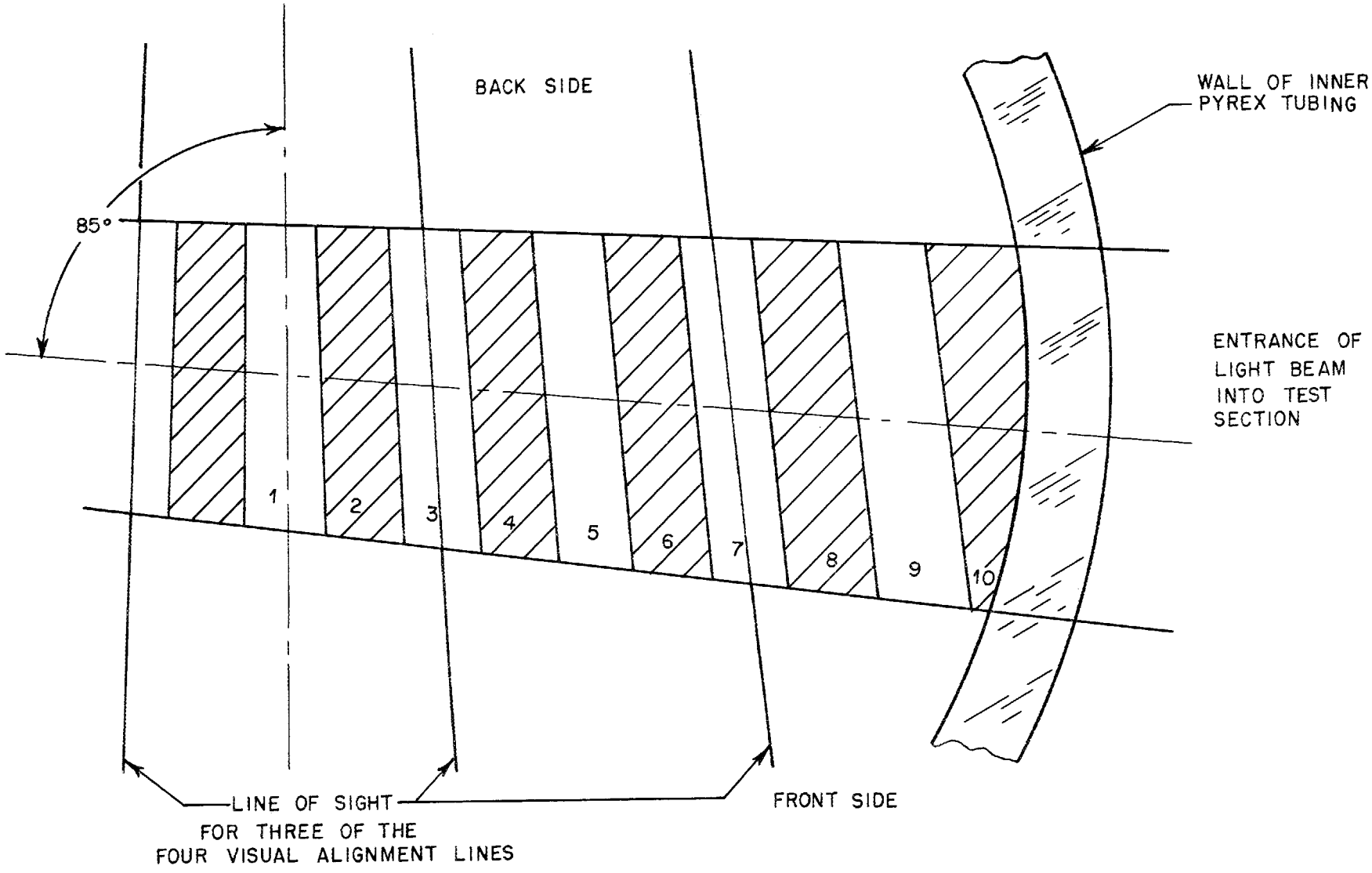

Fig. 19. Light Beam in Right Half of Test Section Showing Compartments

in view of the instruments and methods used. The individual velocity measurements were estimated to be in error by no more than 15 percent; the error in the average velocity for a compartment was probably less. With the timing distance chosen equal to one inch a beam width of 0.2 d was necessary so that approximately half of the droplets chosen at random would traverse the entire timing length before disappearing from sight due to turbulent components. This condition was met for the case of Data Set E; for the other Data Sets the turbulence was less and fewer than half of the droplets chosen disappeared from view within the timing distance. Since the radius and the velocity vary over a wide range within each compartment, one must make a number of velocity observations and, by some statistical method obtain a unique velocity and radius for each compartment which, when plotted, will fall on the true velocity versus radius profile curve that was present during the experiment. It was decided that a minimum of 20 velocity measurements would be taken for each compartment. For seven of the points plotted in the velocity profiles there were less than 20 observations made; these points were for compartments 1, 2, and 3 where the light intensity was low and observations were more difficult to make. In many cases more than 20 observations were made in a compartment. The combined effects of the excess reflected light from the right wall of the Pyrex pipe and the relatively large amount of refraction near that wall raised serious doubt concerning the randomness of the data from compartment 10 so they were not used in any of the Data Sets except E. For Data Set E the data for compartments 9 and 10 were inadvertently combined so these data were treated as compartment (9-10) data.

It was decided to use the arithmetic average of the experimentally observed velocities as the representative or unique velocity for that compartment. Stated mathematically, for n observations in the ith compartment the average velocity is:

$$\overline{u_i}(n) = \frac{1}{n} \sum_{j=1}^{n} u_j \quad \ldots\ldots\ldots\ldots\ldots \quad (21)$$

Let $G_i(u)$ du represent the fraction of the droplets in the ith compartment having axial velocity components between u and u + du if an infinite number of observations had been made. If u_a and u_b represent the minimum and maximum velocities, respectively, in the ith compartment then the average velocity is:

$$\overline{u_i} = \int_{u_a}^{u_b} u\, G(u)\, du \quad \ldots\ldots\ldots\ldots \quad (22)$$

obviously

$$\overline{u_i} = \lim_{n \to \infty} \overline{u_i}\,(n) \quad \ldots\ldots\ldots\ldots\ldots \quad (23)$$

In this report it was decided to use a value of n equal to 20. In analyzing the data it is assumed that:

$$\overline{u_i} = \overline{u_i}\,(20) \quad \ldots\ldots\ldots\ldots \quad (24)$$

The velocity ranges in the various compartments for two typical runs are shown in Table IV.

The remaining problem is to calculate the value of $\overline{R_i}$ that is correct to use in plotting $\overline{u_i}$. Let $F_i(R)$ dR represent the fraction of the droplets in the

TABLE IV

MINIMUM AND MAXIMUM VELOCITIES OBSERVED IN A COMPARTMENT FOR TWO TYPICAL RUNS

Compartment Number i	Number of Observations n	Velocity $\overline{u_i}$	Velocity Range in percent of $\overline{u_i}$
Run No. 7 - Data Set B			
1	22	34.5	53 - 241
2	24	55.8	50 - 154
3	29	57.6	62 - 152
4	20	74	77 - 131
5	24	73	75 - 137
6	26	74.4	77 - 127
7	21	80	68 - 120
8	33	69.6	66 - 130
9	22	48.6	58 - 136
Run No. 12 - Data Set E			
1	24	130.2	64 - 192
2	23	150	69 - 133
3	23	158.4	63 - 146
4	24	185.6	73 - 145
5	26	181	57 - 166
6	22	186.4	73 - 147
7	22	179.2	57 - 140
8	32	173.6	64 - 144
9-10	43	104.2	43 - 161

ith compartment having a radial position between R and R + dR if an infinite number of observations are made.

Then

$$F_i(R)dR = G_i(u)\ du \quad \ldots\ldots\ldots\ldots \quad (25)$$

and

$$\int_{R_a}^{R_b} F_i(R)dR = \int_{u_a}^{u_b} G_i(u)\ du = 1 \quad \ldots\ldots\ldots \quad (26)$$

Now let it be postulated that the velocity profile can be satisfactorily represented by a linear function within the bounds of each compartment or:

$$u = C_4 + C_5\ R \qquad \text{for } R_a < R < R_b \quad \ldots\ldots\ldots \quad (27)$$

For small compartments this is permissible. Combining (25), (26), and (27), get:

$$C_4 + C_5\ \overline{R_i} = \int_{u_a}^{u_b} (C_4 + C_5\ R)\ F(R)dR$$

$$\overline{R_i} = \int_{R_a}^{R_b} R\ F_i(R)dR \quad \ldots\ldots\ldots\ldots \quad (28)$$

Presuming a random distribution and choice of droplets, let it be postulated that the probability that a given droplet, observed to be in the ith compartment, is in the elemental area R dR dω is equal to a distribution factor, ξ , times

the ratio of the area of the elemental area to the area of the ith compartment. Thus:

$$\left(F_i(R)\right)_{\xi} \, dR = \frac{R \int_{\omega_a}^{\omega_b} \xi \, d\omega \, dR}{\int_{R_a}^{R_b} R \int_{\omega_a}^{\omega_b} \xi \, d\omega \, dR} \quad \ldots\ldots\ldots\ldots (29)$$

If the flow had been perfectly streamline a value for ξ equal to unity would be correct. In the experiment many of the droplets did not traverse the measuring distance before disappearing from view outside the beam. This suggests that the probability of obtaining the velocity of droplets was greater for locations in the center of the beam than for those near the edge of the beam. This effect can be represented by a linear form of ξ that is equal to unity at the center of the beam and equal to zero at the edges of the beam.

The values of $\overline{R_i}$ were computed by integration of equations (29) and (28) for the geometry of the light beam as obtained from a refraction analysis. It was believed that the two values of ξ, which will be called, $\xi = 1$, and ξ-linear represent extremes which bound the value of $F_i(R)$ and $\overline{R_i}$ desired. Thus, the values of $\overline{R_i}$ used, which appear in the last column of Table V, were the result of the average of $\overline{R_i}$ ($\xi = 1$) and $\overline{R_i}$(ξ-linear).

TABLE V

MEAN RADII FOR LIGHT BEAM COMPARTMENTS

Compartment (see Fig. 19)	Range of R at Centerline of Beam	Total Range of R	$\overline{R_i}(\xi = 1)$	$\overline{R_i}(\xi\text{-linear})$	$\overline{R_i}$ used
i = 1	0 to 0.05	0-0.208	0.108	0.078	0.093
2	0.05 to 0.15	0.05-0.265	0.152	0.130	0.141
3	0.15 to 0.25	0.15-0.353	0.235	0.218	0.227
4	0.25 to 0.35	0.25-0.443	0.328	0.317	0.322
5	0.35 to 0.45	0.35-0.538	0.424	0.411	0.418
6	0.45 to 0.55	0.45-0.638	0.523	0.515	0.519
7	0.55 to 0.65	0.55-0.745	0.622	0.616	0.619
8	0.65 to 0.767	0.65-0.855	0.732	0.725	0.728
9	0.767 to 0.884	0.767-0.975	0.848	0.841	0.844
10	0.884 to 1.0	0.884-1.000	0.950	0.946	0.948
9+10	0.767 to 1.0	0.765-1.000	0.894	0.890	0.892